Impact of 10 January 1997 geomagnetic storm on the nighttime Weddell Sea Anomaly: A study utilizing data provided by the TOPEX/Poseidon mission and the Defense Meteorological Satellite Program, and simulations generated by the Coupled Thermosphere/Ionosphere Plasmasphere model

Ildiko Horvath[1]

Received 2 November 2006; revised 13 March 2007; accepted 5 April 2007; published 30 June 2007.

[1] This study investigates the evolution of 10 January 1997 magnetic storm and the nighttime space weather change created by the impact of the interplanetary shock wave and associated events on the ionosphere. Its aims are to trace the storm's energy flow dissipation and transportation processes and to learn about the response of nighttime ionosphere to these interplanetary events, focusing on the reaction of the nighttime Weddell Sea Anomaly (WSA). To track down the consequential space weather changes, multi-instrument measurements and Coupled Thermosphere/Ionosphere Plasmasphere (CTIP) simulations were combined. As results show, the first response of nighttime WSA to the energy input in the magnetosphere, when B_Z turned southward, was its ~50% total electron content (TEC) and Ni increase maintained during the main phase, indicating long-duration positive storm effects. At ~0800 universal time (UT) the second such B_Z event triggered the depletion of equatorial and northern midlatitude ionosphere, a signature of strong downward E × B plasma drift, and launched gravity waves. Following a period of very bright aurora, at ~1200 UT, some southern midlatitude and subauroral plasma enhancements developed. TOPEX detected an enhancement between 45–65°S (dip), where the equatorward winds were most effective, with a sudden TEC drop-off, a signature of the plasmapause. Particularly strong negative storm effects depleted the nighttime WSA's TEC-Ni (~45–50%) and O/N_2 ratio (~21%). The Bent model could simulate the WSA, but not the storm-related ionospheric responses. CTIP simulations indicated equatorward winds causing downwellings and changes in the neutral atmospheric composition revealed by the O/N_2 ratio. Joule heating and electric fields were the major geophysical factors observed changing space weather during this storm.

Citation: Horvath, I. (2007), Impact of 10 January 1997 geomagnetic storm on the nighttime Weddell Sea Anomaly: A study utilizing data provided by the TOPEX/Poseidon mission and the Defense Meteorological Satellite Program, and simulations generated by the Coupled Thermosphere/Ionosphere Plasmasphere model, *J. Geophys. Res.*, *112*, A06329, doi:10.1029/2006JA012153.

1. Introduction

[2] Geomagnetic storms are large disturbances in the Earth's magnetosphere created by the disturbed solar wind from coronal mass ejections (CMEs) that compresses the Earth's magnetosphere while depositing considerable amounts of energy directly into the upper atmosphere. Ionospheric storms are driven by that direct energy input, which takes place in the forms of enhanced electric fields, currents, and energetic particle precipitation [*Buonsanto*, 1999].

[3] To describe the major events of 6–11 January 1997: they began with an Earth-directed CME, continued with a geomagnetic storm that was followed by a substorm, and finished with declining magnetic activity. Although this geomagnetic storm carried all the typical observational signatures characteristics of a space storm, these events are special even today since the International Solar Terrestrial Physics (ISTP) mission tracked their progress from the Sun to the Earth in near real time. With a full fleet of ISTP satellites and ground-based observatories, providing a large variety and wealth of data, a collaborative analysis of these events had been carried out by the space science community as a coordinated effort. Via total electron content (TEC) measurements from more than 150 ground-based GPS stations, the process of ionospheric storm evolution was tracked and detailed TEC pictures became available almost in real time. Significant morphological features observed in the global GPS TEC data were reported by *Ho et al.* [1998]. Over Europe and part of the North American continent,

[1]School of Information Technology and Electrical Engineering, Electromagnetics and Imaging, University of Queensland, Brisbane, Queensland, Australia.

Copyright 2007 by the American Geophysical Union.
0148-0227/07/2006JA012153

Jakowski et al. [1999] investigated the main phase of the storm and observed large deviations from the average storm behavior particularly at high latitudes on the late night/early morning longitude sector. *Mikhailov and Forster* [1999] analyzed storm effects and possible physical mechanisms with the Millstone Hill incoherent scatter facility and concluded that daytime NmF2 negative storm effects were caused by the decrease of $O/(N_2 + O_2)$ ratio, and that the $E \times B$ drift controlled the mechanisms of plasma compression and decompression. Because of the good data coverage, the interval of 6–11 January 1997 was chosen as a CEDAR (Coupling, Energetics, and Dynamics of Atmospheric Regions) storm period for coordinated analysis [*Buonsanto et al.*, 1999].

[4] The nighttime and daytime space weather features of the Weddell Sea Anomaly are the manifestation of the so-called Weddell Sea Anomaly phenomenon discovered by *Penndorf* [1965]. It is characterized by a uniquely inverted equinox/summer diurnal electron density pattern wherein the maximum develops at nighttime and the minimum at daytime. These peculiarities of the F2 layer were reviewed by *Dudeney and Piggott* [1978], first detected in the TOPEX/Poseidon radar data by *Horvath and Essex* [2003], and further investigated by *Horvath* [2006; I. Horvath, A TOPEX TEC climatology study of the daytime Weddell Sea Anomaly coupled with Bent model and Coupled Thermosphere/Ionosphere Plasmasphere model (CTIP) simulations, unpublished manuscript, 2007, hereinafter referred to as Horvath, unpublished manuscript, 2007a]. As is well known today, their development can be attributed to the combination of various geophysical factors. These are the large offset between the geographic and magnetic poles, the interesting magnetic field line configuration due to the Earth's tilted axis in this unique polar environment, the thermospheric neutral winds that are equatorward directed at night and blow poleward during the day, and the solar illumination that lasts 24 hours a day during summer [*Dudeney and Piggott*, 1978]. With space-based radar altimetry, the development of both features mostly west of the Weddell Sea was first revealed by *Horvath and Essex* [2003]. These researchers also first noted the appearance of the anomaly over a much larger area than was previously thought by other researchers on the basis of their ground-based ionosonde measurements. The anomaly's continuation at latitudes higher than 66°S (geographic), which is the limit of the TOPEX/Poseidon data coverage, was indicated by *Horvath* [2006, unpublished manuscript, 2007a]. The large offset between the centers of the daytime and nighttime features was first observed also by Horvath (unpublished manuscript, 2007a).

[5] Although the various aspects of 6–11 January 1997 events have been thoroughly researched and extensively documented in a large volume of published literature, the nighttime Weddell Sea Anomaly's response to these events has not been investigated at all. Further, modern space-based instruments have not been utilized to study ionosphere dynamics in terms of positive and negative storm phases. Furthermore, the ability of models including modern coupled models has not been tested in reproducing the nighttime Weddell Sea Anomaly during a storm. This paper intends to reveal the response of the nighttime Weddell Sea Anomaly and of other ionospheric regions to the 6–11 January 1997 events, and to evaluate two models in reproducing the nighttime ionosphere during these events. These models are the Coupled Thermosphere/Ionosphere Plasmasphere (CTIP) model and the Bent model. To succeed, a wider period (6–13 January) was examined with experimental data, and a narrower period was studied (9–12 January) via model simulations. In detail, the morphology of nighttime electron and ion density distribution was experimentally researched by utilizing data from space-based remote sensing and in situ plasma measurements. The TOPEX/Poseidon radar altimeter provided over-the-ocean TEC values. In situ plasma measurements supplied by the Defense Meteorological Satellite Program (DMSP)-F12 spacecraft were analyzed for the characteristics of the plasma environment in the Weddell Sea Anomaly region and elsewhere, and for quiet time and storm-related ionosphere dynamics in terms of positive and negative storm phases. Storm-related ionosphere dynamics were also related to magnetospheric and solar wind perturbations. For obtaining over-the-ocean TEC simulations, the Bent climatology model was employed. Meanwhile, the CTIP simulations also helped to explain some storm-time variations, as the CTIP model is also an excellent tool providing a better understanding of their underlying physical mechanisms.

2. Instrumentation and Measurements

2.1. TOPEX/Poseidon

[6] Sea surface topography from space is the essence of TOPEX/Poseidon. It is a highly successful and ambitious mission that has been operating since August 1992 and widely used for ionospheric research. This dual-frequency (f_{Ku} = 13.8 GHz, f_C = 5.6 GHz) instrumentation operating at 1335 km in the F2 layer provides direct vertical height measurements ($\partial\Delta P'$) for obtaining unambiguous total electron content or TEC values. For convenience, the TEC unit is utilized for TEC values where 1 TECU = 10^{+16} e^-/m^2 [*Imel*, 1994]. TEC is the integral of electron density along the line of sight between the satellite (S) and the subsatellite reflection point (R; see equation (1)) on the surface of the ocean. A detailed description of the procedure developed for obtaining TOPEX TEC values from the radar altimeter data is given by *Horvath* [2006, unpublished manuscript, 2007a]:

$$\text{TOPEX TEC} = \int_R^S \text{Nds} = -\frac{f_{Ku}^2}{403.1}\delta\Delta P' \qquad (1)$$

where N = electron density (e^-/m^3) and ds = element of height (m).

2.2. Wind

[7] NASA's Wind satellite started its solar wind monitoring mission as part of the Global Geospace Science (GGS) initiative and ISTP project in 1994 with a goal to study the interplanetary magnetic field (IMF), particularly near the magnetospheric bow shock and magnetopause regions, plus the properties of solar wind. On a highly elliptical orbit where the dayside apogee is between 80 and 230 Earth radii (R_e), the Wind satellite carries an array of 8 scientific instruments for measuring the charged particles, and the electric and magnetic fields of the interplanetary medium

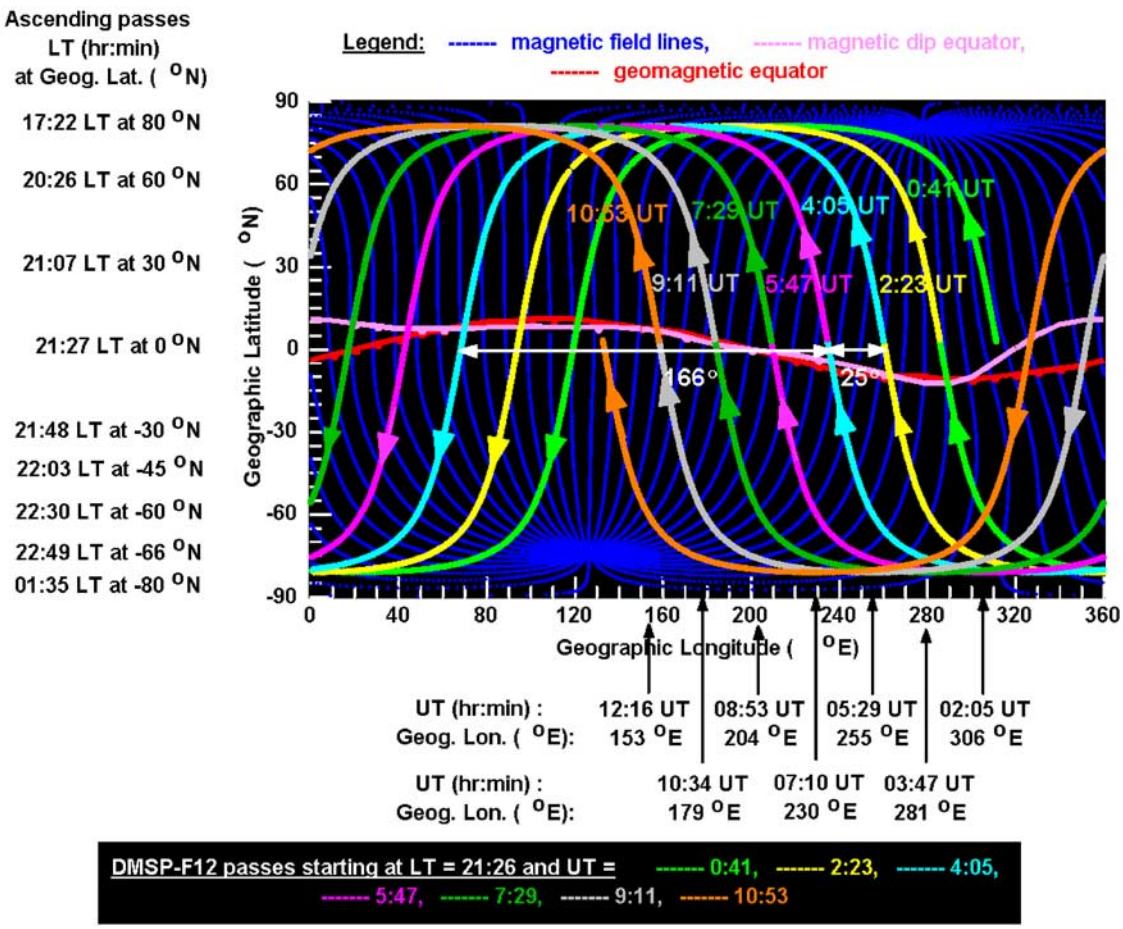

Figure 1. Some ground tracks of the Defense Meteorological Satellite Program (DMSP)-F12 spacecraft are illustrated with the magnetic field lines and geomagnetic and magnetic dip equators in the grid of geographic parallels. For the ascending passes the local time variations with geographic latitude and the universal time variations with geographic longitude are demonstrated. As the LT and UT values indicate, a longitudinal space weather feature detected at different UT during different passes along certain geographic latitude can be viewed at a single local time.

that characterize the near-Earth plasma environment. During the first 2 years of operation, Wind was positioned in a sunward, multiple double-lunar swing-by orbit. This was followed by a halo orbit at the Earth-Sun Lagrangian liberation point, L1, which is positioned between the Sun and the Earth ($\sim 1.5 \times 10^6$ km from the Earth) and lies on a straight line connecting the Sun and the Earth [*Harten and Clark*, 1995]. This considerable distance creates a time lag of 30 min minimum and 1 hour maximum that must be considered when Wind data are compared to ground based measurements. For this study, the 92-s resolution measurements of magnetic field component (B_X, B_Y, and B_Z; in nT) computed in Geocentric Solar Ecliptic (GSE) coordinates and of solar wind velocity (V_{SW}; in km/s) were obtained from the Wind database.

2.3. DMSP

[8] The Defense Meteorological Satellite Program (DMSP) has been operational since 1965. Its primary mission of imaging the Earth in white and infrared lights for weather forecasting was extended to space environmental monitoring when later spacecraft carrying SSJ4/5 particle and fields detectors were launched. These spacecraft sample the ionospheric plasma at an altitude of about 850–870 km, and are in near-polar and circular orbits. Their orbital inclination is 96 degrees keeping their orbits fixed in local time (see details below). There are at least two spacecraft operational at any given time, one in the dawn-dusk sector and one in the early evening/early morning sector [*Hairston et al.*, 1997].

[9] DMSP data used in this study were from the F12 spacecraft that is one of the seven current DMSP series. F12 orbits the Earth in the 0928–2128 local time (LT) sector with a period of 101 min. Thus its data are suitable for investigating the nighttime Weddell Sea Anomaly, detected at ~2100 LT in the TOPEX data, and for making comparisons with the TOPEX TEC passes. Like any other DMSP spacecraft, the F12 spacecraft completes 14 orbits each day. Each orbit is made up of an ascending and a descending pass. In Figure 1, the first seven orbits of F12 are plotted with the magnetic field lines, and with the geomagnetic and magnetic dip equators in the grid of geographic parallels. As the map shows, each orbit crosses over the two hemispheres between ±81°N geographic latitudes. Two adjacent ascending

or descending passes are separated by ~25° (geographic longitude), while ascending and descending passes of the same orbit are 166° apart. Some local time and universal time values of the displayed ascending passes are listed for a few geographic latitudes and longitudes, respectively. Figure 1 demonstrates how the local time remains constant along the geographic latitude, and how the local time changes with geographic latitude while the universal time changes with geographic longitude. According to these LT and universal time (UT) characteristics of the DMSP data, longitudinal space weather features detected along certain geographic latitude can be viewed at a constant local time.

[10] All DMSP spacecraft continuously record from four instruments that are part of the Special Sensor Ions, Electrons and Scintillation (SSIES) package onboard. This package contains the Langmuir Probe (LP), Retarding Potential Analyzer (RPA), Ion Drift Meter (DM), and Scintillation Meter (SM). For this investigation, 4-s resolution data files containing DM, RPA, and LP data were utilized. Measurements of plasma flow components (Vx, Vy, Vz), plasma ion density (Ni in ions/cm^3), fractional composition of the plasma (H^+, O^+, He^+), and electron and ion temperatures (Te and Ti in °K) are listed in the DMSS SIESS database. Further, UT, MLT, and spacecraft location in geographic and geomagnetic coordinates are also given.

2.4. Magnetometers

[11] Geomagnetic data provide background information on daily solar activity and its impact on the geospace environment. Geomagnetic perturbation indices can be used to quantify the magnitude of geomagnetic storms because of the geoeffective nature of CMEs that drive all large magnetic storms and their attendant effects, such as auroral displays. As *Davis et al.* [1997] explained, a geoeffective nature indicates an ability to significantly perturb the Earth's environment. In this study, the most widely used Auroral Electrojet (AE), Disturbance storm time (Dst), and *Kp* geomagnetic perturbation indices were employed.

3. CTIP and Bent Model Utilized for Simulations

[12] Two modern models, the CTIP model and the Bent model, provided simulations for the period 9–12 January inclusive. The CTIP model is a physical, self-consistent computational model that reproduces well the key processes taking place in the thermosphere. It consists of three distinctive components: a global thermospheric model, a high-latitude ionosphere model, and a low- and midlatitude ionosphere/plasmasphere model. As described by *Fuller-Rowell et al.* [1996b] and *Millward et al.* [1996], CTIP solves the 3-D time-dependent equations of momentum, energy, and continuity for neutral particles and ions. As such, it is one of the most comprehensive coupled models currently available. CTIP simulations can be requested online. For this study, data for 4 days were simulated by one continuous run. The Bent model is a comprehensive empirical climatology model that has been extensively used for ionospheric calibrations and predictions. Since it is based on averaged past observations, spanning a significant part of the solar cycle, the Bent model fits the ionospheric TEC measurements well over long timescales [*Ho et al.*, 1998]. In the TOPEX/Poseidon database, ionospheric height corrections estimated by the Bent model are listed with the experimental measurements. Thus the Bent model TEC values can be extracted from the radar data by applying the same procedure developed for obtaining experimental TOPEX TEC values.

4. Description of the 6–13 January 1997 Events

[13] According to SOHO/LASCO [*Fox et al.*, 1998; *Ho et al.*, 1998; *McEwen et al.*, 1999], an Earth directed CME left the Sun at 1734 UT on 6 January 1997. To track its passage through the interplanetary medium, the Wind data were used. For the period of 6–13 January 1997, the B_X; B_Y; and B_Z components of the IMF, and the total magnitude of the solar wind velocity (V_{SW}) are shown in Figure 2. Among the IMF components, the north–south or B_Z component is the most important influence on the magnetosphere, as B_Z controls the fraction of the energy in the solar wind flow that is extracted by the magnetosphere [*Davis et al.*, 1997]. As the CME took 4 days to travel through the interplanetary space before arriving on Earth, there was a magnetically quiet period between 6 and 9 January when all three B components were consistently close to zero. Driven by the CME and preceding the magnetic cloud. which is a subset of CME, a sudden increase of solar wind from 350 km/s to 430 km/s at ~0010 UT on 10 January was the first signature of the interplanetary shock [*Fox et al.*, 1998]. After a 4-hour period of high solar wind dynamic pressure, at ~0400 UT, the second sudden intensification of the solar wind to ~480 km/s marked the arrival of the cloud [*Fox et al.*, 1998]. This impulsive change in the solar wind velocity was the signature of an interplanetary shock wave in the vicinity of the Earth that triggered the primary storm sudden commencement (indicated as 1st SSC in Figure 2) at ~0442 UT. *Smith et al.* [1986] pointed out first and *Lepping et al.* [1995] reinforced later that an SSC is also the ground manifestation of a strong magneto-hydrodynamic wave transmitted to the Earth around the onset of a magnetic storm.

[14] At around the time of 1st SSC, the Wind spacecraft was ~70 R_E upstream. It detected the first shock wave at 0050 UT on 10 January and revealed the arrival of a magnetic cloud with the direction change of the IMF component of B_Z from northward to southward that remained southward directed for 12 hours from 0440 UT onward (see Figure 2). It is known that high solar wind speeds and prolonged intervals of strong southward directed B_Z component are the signature of the energy having coupled efficiently, and is transferred to the Earth's magnetosphere and upper atmosphere from the solar wind This energy transfer takes place primarily via reconnection between the IMF and the terrestrial magnetic field at the dayside magnetopause [*Gosling*, 1993; *Buonsanto and Fuller-Rowell*, 1997]. First suggested by *Dungey* [1961], this reconnection produces open field lines, which allow mass, energy and momentum to be transferred [*Davis et al.*, 1997].

[15] Figure 2 demonstrates that the magnetic storm started intensifying after the initial positive Dst phase. A negative main storm phase occurred between 0600 and 1000 UT displaying a minimum Dst of −81 nT and a maximum *Kp* of 7. This was followed by a slow recovery phase. As the magnetic cloud passed the Wind spacecraft during the main and recovery periods, the IMF slowly rotated to a northward orientation. This event can be seen in the B_Z data. Early on

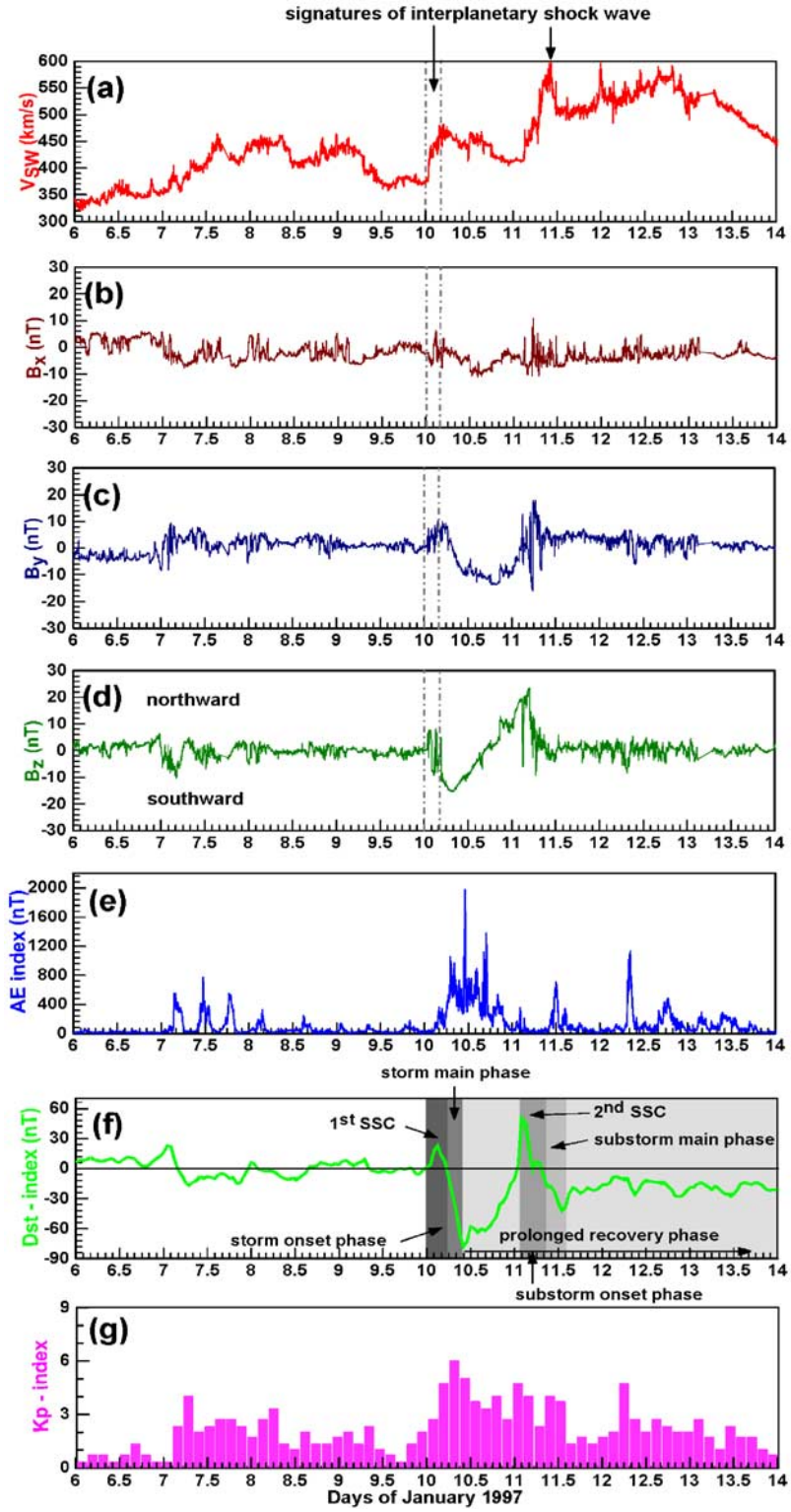

Figure 2. (a) Solar wind speed (V_{SW}) and (b)–(d) interplanetary magnetic field component (B_X, B_Y, B_Z) variations during the studied period were monitored by utilizing the Wind satellite data. Geomagnetic indices of (e) Auroral Electrojet (AE), (f) Disturbance storm time (Dst), and (g) *Kp* are utilized to identify the various storm phases during the studied period. The vertical lines indicate events of sudden solar wind increase that are the signatures of interplanetary shock waves.

11 January, the end of the cloud was observed, implying a structure 30 million miles wide [*Fox et al.*, 1998]. This slow recovery process was interrupted when the cloud's magnetic field rotated to a strongly northward direction ($B_Z \approx +25$ nT), decreasing the solar wind to ~410 km/s, and created a large pressure pulse that struck an already loaded magnetosphere with such a force that was sufficient to shift the magnetopause to within geosynchronous satellite orbit [*Fox et al.*, 1998]. Such an event occurring when the IMF is strongly southward is not unusual [*Rufenach et al.*, 1989], but when B_Z is northward it is quite unusual. According to up-to-date knowledge, this was the first event observed with strong northward detected IMF. While the B_Z component decreased to zero, the solar wind increased to 600 km/s, creating a substorm. Its SSC is labeled as 2nd SSC in Figure 2. This event disrupted and prolonged the storm's recovery phase characterized by declining magnetic activity.

5. Nighttime Ionosphere During the 6–13 January Events

5.1. TOPEX TEC, DMSP-F12 Ni, Bent Model TEC, and CTIP NmF2 Maps

[16] In Figure 3 (left), a series of eight nighttime TOPEX TEC maps constructed with color-coded passes for the extended 6–13 January period of the storm events is shown. These maps depict the temporal variation of the nighttime ionosphere before (6–9 January), during (10–11 January), and after (12–13 January) the storm. Their most significant feature is the nighttime Weddell Sea Anomaly appearing as a large plasma peak. The anomaly's response to the magnetic events is exhibited by its strong enhancement in TEC during the storm main phase that was followed by its even stronger depletion in TEC during the recovery phase. These TOPEX TEC maps also illustrate that in other latitude and longitude regions, the nighttime ionosphere had a less obvious reaction to the storm events possibly because of the generally low TEC levels.

[17] For a shorter period, 9–12 January, the nighttime ionosphere, remote sensed by the plasma ion density (Ni) measurements of the DMSP-F12 spacecraft, is illustrated in Figure 3 (top, right). In the Weddell Sea Anomaly region, where the TOPEX LT and DMSP-F12 LT are very similar (~2200) at ~55°S (geographic), the structures of the ionization detected in the two types of data are very similar. In other latitude regions such as at the equator or in the entire Northern Hemisphere, where the TOPEX and DMSP LT values are different, the TEC and Ni maps cannot be compared directly. A normal nighttime plasma distribution can be observed in the first Ni map of 9 January. After the storm began, DMSP-F12 detected some storm-related large equatorial enhancements in the Australian region on 10 January, besides the intensification of the nighttime Weddell Sea Anomaly. On the following day, 11 January, the TEC depletion of the nighttime ionosphere was obvious except north of the Weddell Sea Anomaly where some TEC enhancements appeared and disappeared on the next day, 12 January (see Figures 3i–3l).

[18] A set of simulated TEC data was produced by the Bent model (see Figure 3 (bottom, right)) and mapped for this shorter period of 9–12 January. Obviously, the Bent model could reproduce the nighttime ionosphere with the Weddell Sea Anomaly very well for the magnetically quiet day of 9 January. Although the simulated TEC values were 50% lower than the TOPEX TEC values, the modeled nighttime ionosphere shows a great resemblance to the quiet time ionosphere remote sensed by TOPEX between 6 and 9 January (see Figures 3a–3d). However, the Bent model could not reproduce any response of the ionosphere to the storm events. Thus the Bent model TEC maps simulated for the main (10 January) and recovery (11 January) phases are quite similar to the quiet time (9 January) map, showing almost no variations (see Figures 3m–3p).

[19] A set of F2 layer (altitude = 250 km) electron density (NmF2) maps was simulated with the CTIP model for this shorter period of 9–12 January (see Figure 4). For a universal time, the 0712:00 value was chosen since 0700 is the UT of the TOPEX and DMSP recordings at ~230–250°E and ~55–70°S where the center of the nighttime Weddell Sea Anomaly is situated (see details in section 5.3). As the CTIP maps show the ionosphere at a constant UT, ~0700, across all longitudes, this high midlatitude region (~230–250°E and ~60–70°S) west of the American longitude sector represents a simulation of the nighttime Weddell Sea Anomaly. Shown by the high NmF2 region there (see Figure 4a), the CTIP model could reproduce the nighttime Weddell Sea Anomaly under quiet magnetic conditions. The anomaly's intensification during the main storm phase (see Figure 4b), its depletion during the recovery phase (see Figure 4c), and its redevelopment on the following day (see Figure 4d) are all obvious. Because of the accuracy of the CTIP model, the thermospheric circulations and the chemical makeup of the neutral air could be studied for the Weddell Sea Anomaly. To do that, a series of simulations was prepared for the prestorm day of 9 January (see Figure 5), so these quiet time values could be compared with storm-time values obtained by further CTIP simulations (see details in section 6). According to the quiet time CTIP model results, the high NmF2 values (see Figure 5a) in this region (~230–250°E and ~60–70°S) are related to the high neutral gas temperatures (indicated as T_n; see Figure 5b) caused by the solar illumination of the F2 layer providing continuous ion productions. Written as Vn_lat by CTIP and represented by arrows, the neutral meridional (north–south) component of the neutral gas velocity (Vn) vectors indicate strong nighttime equatorward directed thermospheric circulations in this region (see Figure 5c). The maximum and minimum Vn vector amplitudes in the north–south direction are also indicated in Figure 5c (top, right). In good agreement with the explanation of *Rishbeth et al.* [2000], these equatorward circulations that are coupled with the overall summer-to-winter circulation, created strong upwellings at higher latitudes (indicated as Vn-IP; see Figure 5d). These lifted the F2 layer up to greater altitudes, indicated by the high HmF2 values (see Figure 5e) and helped to maintain the high NmF2 via the low recombination rates. Indicated by the particle number density (N) simulations, the intense vertical motion changed the chemical makeup of the neutral air composition to rich both in nitrogen (indicated as N_N_2; see Figure 5f) and in oxygen (indicated a N_O_2; see Figure 5g), and caused their departure from the chemical equilibrium. As a result, the overall O/N_2 ratio decreased (see Figure 5h).

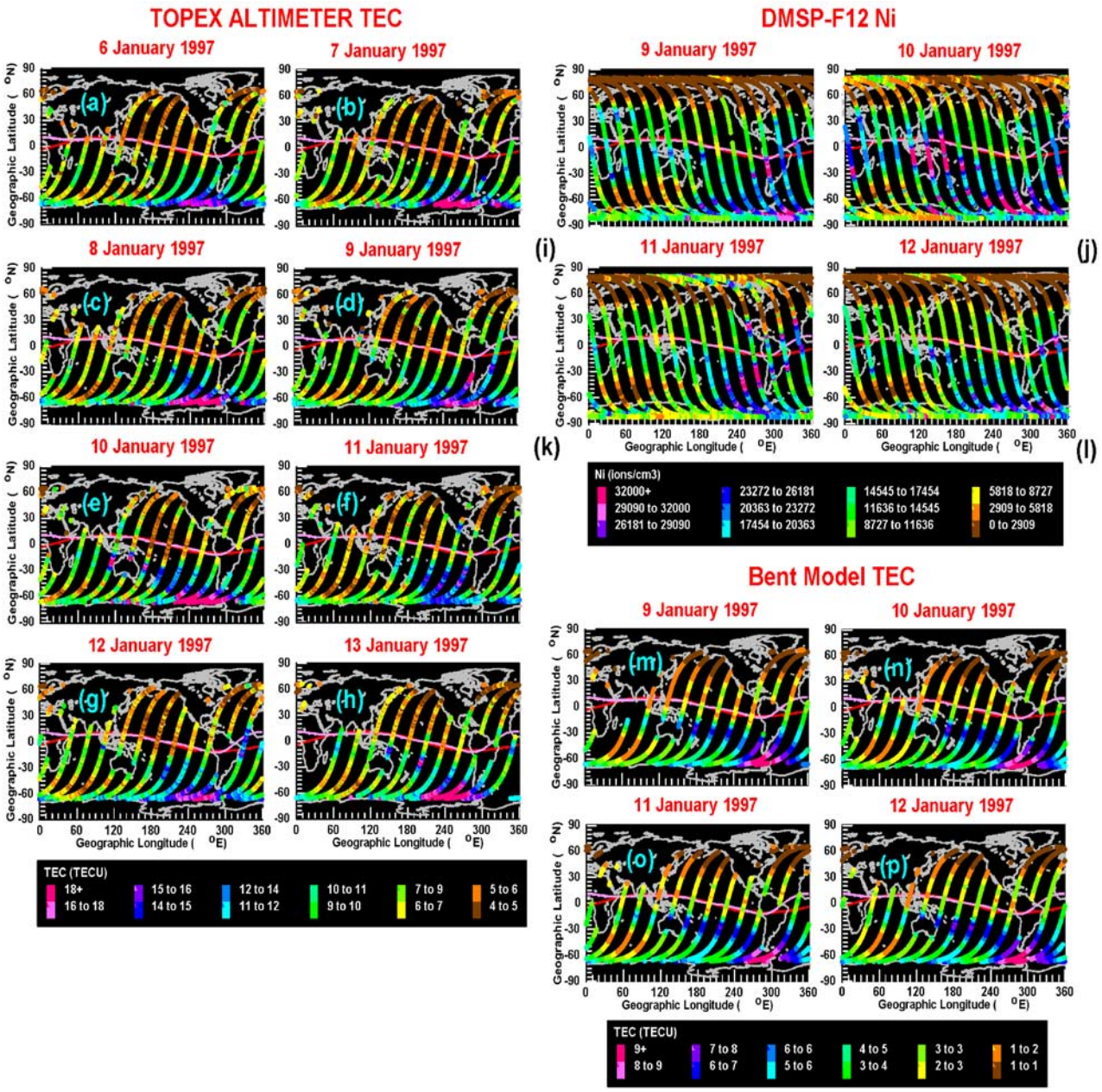

Figure 3. (left) A series of color-mapped TOPEX total electron content (TEC) plots shows the variation of nighttime ionosphere before (6–9 January), during (10 January), and after (11–13 January) the magnetic storm of January 1997. (top right) A series of color-mapped DMSP-F12 Ni plots shows the variation of nighttime ionosphere before (9 January), during (10 January), and after (11–12 January) the magnetic storm of January 1997. (bottom right) The Bent model TEC maps illustrate the success of reproducing the nighttime ionosphere with the Weddell Sea Anomaly during the quiet day and the failure of reproducing any storm-related variations.

[20] In the following sections, the TOPEX TEC and DMSP Ni maps will be analyzed with line plots and DMSP spectrograms in order to describe the prestorm conditions (section 5.2), and to trace the geomagnetic storm's energy flow dissipation and transportation processes in the nighttime ionosphere (section 5.3).

5.2. Prestorm Conditions

[21] Prestorm conditions were investigated in the absence of magnetic disturbance during the period of 6–9 January. These quiet conditions can be viewed in the first four TOPEX TEC maps (see Figures 3a–3d) and in the first Ni map (see Figure 3i). Because of the similar observational capabilities of the two space-based instruments carried by TOPEX/Poseidon and DMSP, the TEC and Ni maps are very similar. According to both instruments, the nighttime Weddell Sea Anomaly appears as a plasma enhancement mainly over the southeastern Pacific. There are differences between the two hemispheres depicted by a highly asymmetric TEC pattern about the magnetic equator. It seems

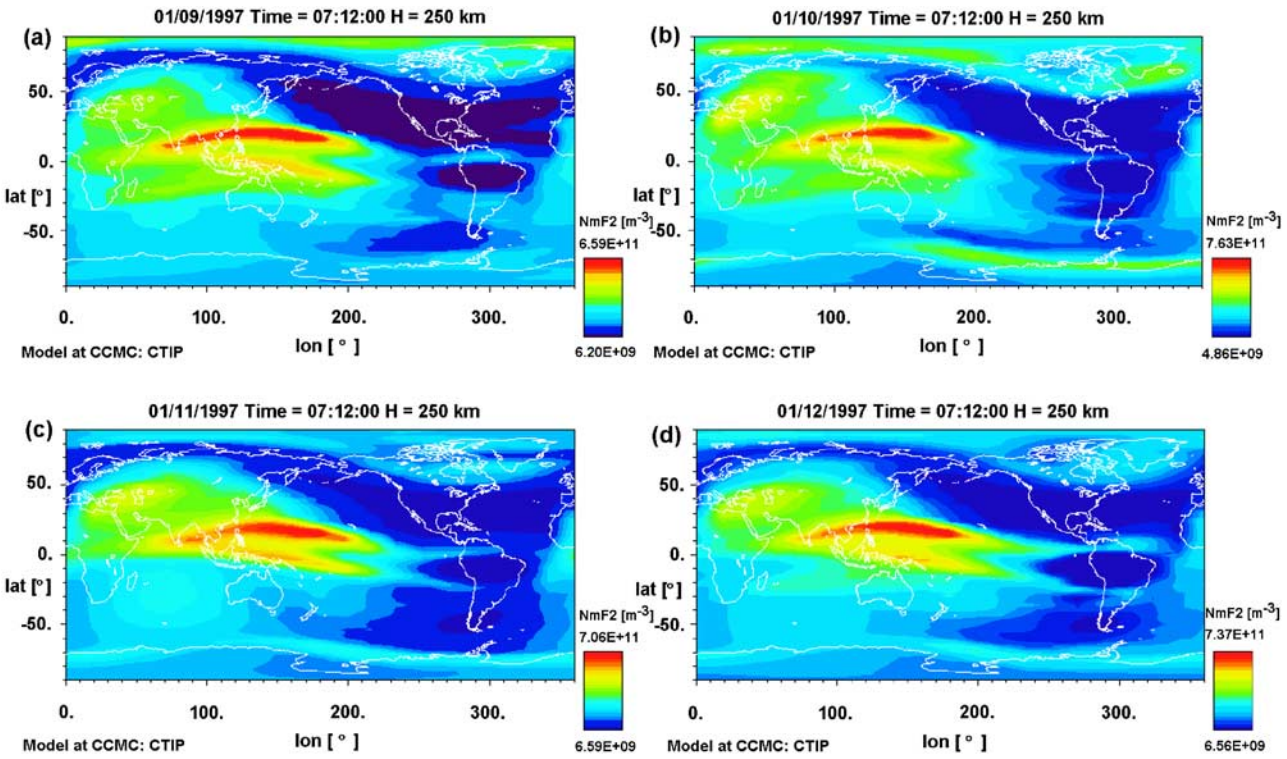

Figure 4. A set of Coupled Thermosphere/Ionosphere Plasmasphere (CTIP) NmF2 maps created for 0712:00 UT depicts the simulations made for the nighttime Weddell Sea Anomaly and for its response to the 10 January storm in the longitude sector of 230–250°E (geographic) at ~2100 LT.

apparent that these differences are due to the main role of magnetic meridional neutral winds in transporting the ionization as a function of inclination, declination and magnetic field strength, and to the combination of southern summer and northern winter at local nighttime. In the southern ionosphere, there is a strong quasi-sinusoidal TEC variation at constant geographic latitude, wherein the TEC peaks over the southeastern Pacific (i.e., the nighttime Weddell Sea Anomaly), becomes depleted over the Indian Ocean (i.e., midlatitude trough). Between these, there are two regions with medium TEC and opposite declination: the southwestern Pacific (eastward declination) and the South Atlantic (westward declination). These four regions define the four longitudinal sectors in the south, namely the Indian, western Pacific, eastern Pacific, and Atlantic [*Horvath*, 2006]. Longitudinal variations are introduced by the declination angles and the field line configuration. In the north, this quasi-sinusoidal variation is very week because there is little variation in declination. Thus the northern nighttime ionosphere over the oceans looks rather undivided longitudinally, like on the TOPEX map constructed for 12 January (see Figure 3g). Inclination introduces latitudinal variations aligned with the magnetic dip equator. Because of the generally low TEC levels in the north, there are also little latitudinal variations in the north making the northern nighttime ionosphere quite uniform. In the south, the latitudinal variation of TEC is more apparent because of the higher levels of ionization. In the recent study by *Horvath* [2006], a very detailed description of the nighttime ionosphere and nighttime Weddell Sea Anomaly during this period is given with the explanation of the underlying physical mechanisms.

[22] For investigating the structures of the quiet nighttime ionosphere on 6 January, a set of line plots are illustrated in Figure 6. As the map shows in Figure 6a, the TOPEX/Poseidon satellite crossed the equator at around 327°E during the pass 239, east of the South American continent, and approached the center of the nighttime Weddell Sea Anomaly up to 66°S where that pass ended. Because the Weddell Sea Anomaly continues at higher latitudes, this TOPEX pass, 239, imaged its equatorward side only (see Figure 6b). At around the same time, the DMSP-F12 spacecraft was sampling the southern ionosphere in this area along its ascending pass from 81°S (geographic) up to the equator (see Figure 6a). During this final ascending lag over the southeastern Pacific, the F12 plasma ion density measurements indicate a latitudinal plasma density profile of the nighttime Weddell Sea Anomaly (see Figure 6c) that is very similar to the one detected by TOPEX (see Figure 6b). By passing the 66°S (geographic) limit of TOPEX data availability, this F12 pass provided direct evidence of the continuation of the nighttime Weddell Sea Anomaly at latitudes higher than 66°S (geographic). It detected the anomaly's peak at around 60°S (geomagnetic) or 70°S (geographic) and its poleward side up to 65°S (geomagnetic) or 81°S (geographic) where the F12 spacecraft turned. At around 65°S (geomagnetic) the ion density drop-off, its position is indicated by the symbol *x*, is the ionospheric signature of the plasmapause. This interpretation was verified by the matching DMSP-F12 spectrogram where the position

of the plasmapause was marked automatically as b0 (see Figure 6g). The first observation of the poleward boundary of the nighttime Weddell Sea Anomaly has recently been reported (I. Horvath, First imaging of the entire nighttime Weddell Sea Anomaly (WSA) using data from DMSP, unpublished manuscript, 2007, hereinafter referred to as Horvath, unpublished manuscript, 2007b). As the two different data plots indicate, the plasma density distribution

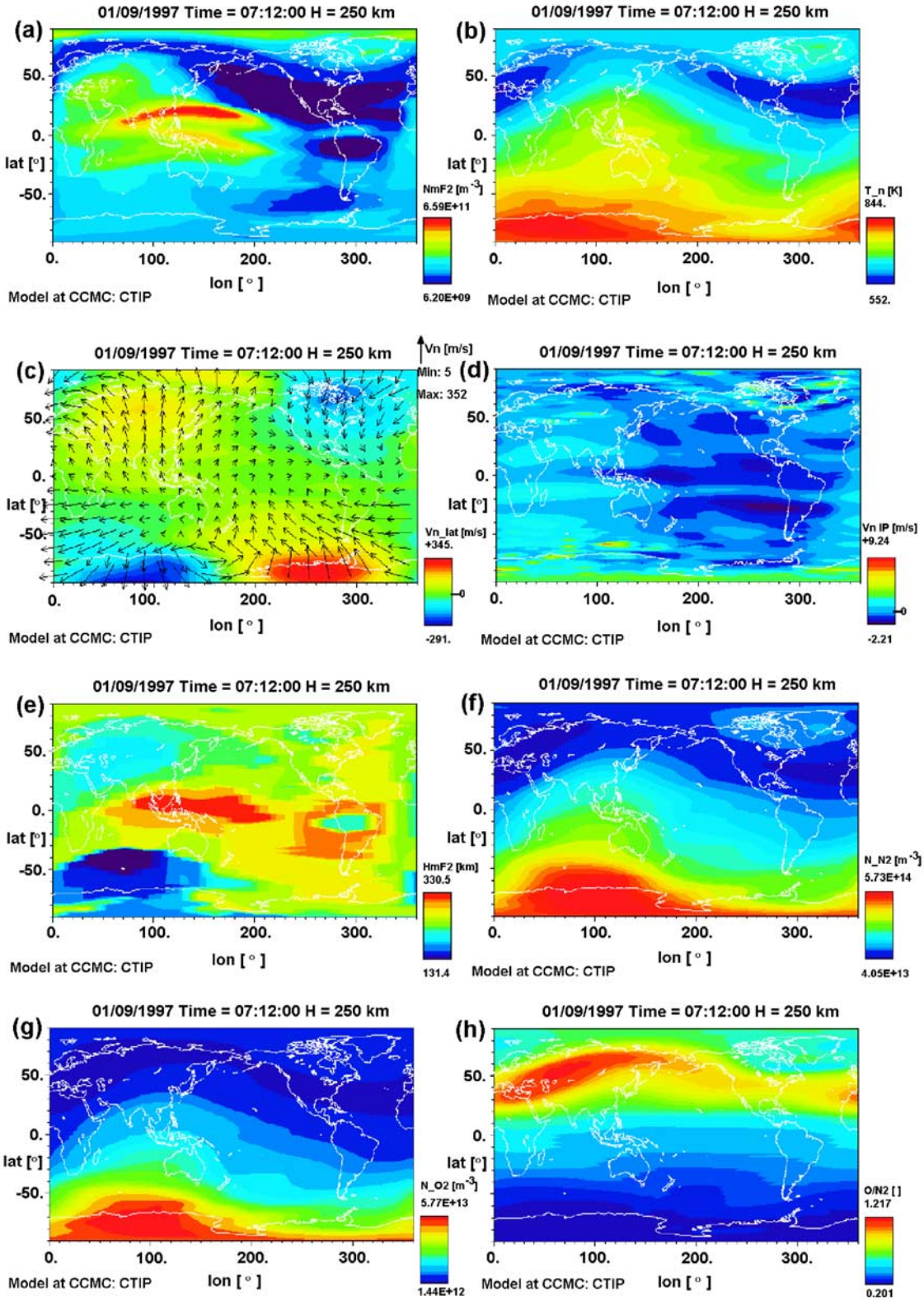

Figure 5

was fairly similar on both sides of the South American continent.

[23] Detected by two TOPEX passes (247 and 249) over the western Pacific, the nighttime electron density distribution was moderately uniform across the two hemispheres, changing only between 5 and 10 TECU (see Figures 6d–6e). In the Australian longitude sector, where high magnetic latitudes are situated at middle geographic latitudes, the TOPEX pass 251 detected at ~1600 UT some plasma enhancements at auroral latitudes (indicated as "A" in Figure 6f). Its location is marked on the map (see Figure 6a) by the symbol *x*. The DMSP-F12 spacecraft orbited this region at around 1500 UT. Its ground track, indicated as F12/A in Figure 6a), crossed the path of the TOPEX pass 251. In Figure 6h, the DMSP-F12 spectrogram depicts structured charged particle precipitation there. On the basis of the automatically marked oval boundaries, a discrete aurora appears between b3a and b5e indicating its equatorward and poleward boundaries, respectively. Equatorward of the discrete aurora (marked as b3a) and poleward of the plasmapause (marked as b0), a diffuse aurora can be identified [*Newell et al.*, 1996]. These aurora images confirm that their ionospheric signature was detected by TOPEX during the pass 251 (see Figure 6f).

5.3. Positive and Negative Storm Features

[24] Storm conditions were investigated during the period of 10–13 January. How the TEC and Ni responded to these conditions can be viewed on the TOPEX (see Figures 3e–3h) and DMSP maps (see Figures 3j–3l). It is important to note that each TOPEX and DMSP pass crosses the equator approximately 2 hours later in UT than the previous pass. Further, those TOPEX and DMSP passes that cross the equator at similar longitudes have similar local times at southern latitudes: at ~50°S (geographic) the local time ~2200 LT. In each TOPEX and DMSP map, the Weddell Sea Anomaly longitude sector from east to west (320–200°E) was detected between 0000–0800 UT. In the latitude range of the Weddell Sea Anomaly (45–66°S), the TOPEX local time varies from 2000 LT to midnight toward the equator. On 10 January, this 0000–0800 UT interval covered part of the storm onset phase that lasted from 0000 UT to 0500 UT, and almost the entire main phase that took place between 0500–1000 UT when B_Z was southward directed. On the following days of 11–13 January, this 0000–0800 UT period covered part of the interrupted section of prolonged recovery phase (i.e., the main phase of the substorm), when the northward directed B_Z reached its maximum on 11 January before it returned to normal.

[25] According to the 10 January maps of TOPEX TEC and DMSP Ni (see Figures 3e and 3j) during the storm onset and main phase, the Weddell Sea Anomaly exhibited a strong positive storm phase. This continued spatially over the southwestern Pacific at 1200 UT and in the Australian longitude sector between 1400–1800 UT during the first 8 hours of the recovery phase on 10 January. On the following day, 11 January, between 0000–0700 UT the Weddell Sea Anomaly exhibited a particularly strong negative storm phase. Later in time, a less intensive negative phase in the Australian longitude sector (1400–1800 UT) and over the Southern Indian Ocean (2000–2400 UT) was detected by TOPEX and DMSP. Whilst the strong negative phase depleted the Weddell Sea Anomaly region, simultaneously some positive features appeared equatorward that gradually faded away as the recovery process progressed during the following days of 12 and 13 January. Some of these storm features will be investigated in the following sections because of their interesting structures and because other journal papers only mentioned them without providing any observational results.

5.3.1. Main Phase

[26] The positive response of the nighttime Weddell Sea Anomaly to the energy input in the magnetosphere was first seen after 0400 UT on 10 January (see Figure 7). This response was indicated by its moderate increase in TEC from ~19 TECU on the quiet day of 6 January (see Figure 6b) to 24 TECU (see Figures 7a–7b) over the same geographic area. 0400 UT is the time when B_Z turned southward (see Figure 2d) and the aurora started intensifying. Its increasing intensification through 0400 UT up to 0725 UT is shown by the AE and *Kp* indices (see Figures 2e and 2g). At around 0700 UT, the AE index dramatically increased to 1050 (nT) from a low of 9 (nT) detected at 0200 UT (see Figure 2e). This marked increase of strong cross-polar-cap potential drop led to the intensification and expansion of the magnetospheric convection electric field encompassing lower latitudes. At the same time, the auroral zone expanded because of the enhanced energetic particle precipitation. These events are the magnetospheric drivers that had a strong effect structuring the high-latitude plasma.

[27] In the Northern Hemisphere, the downward looking TOPEX detected an auroral enhancement at around 0600 UT on 10 January (see Figure 7b) over the Atlantic Ocean. Later on that day, it moved westward and equatorward (see Figure 7c). Their locations are marked by the symbol *x* on the map of Figure 7a and in Figures 7b and 7c. At the same time, the equatorial nighttime ionosphere became depleted as the TEC dropped from the quiet time 10 TECU down to 7.5 TECU (see Figure 7c), indicating an approximate 25%

Figure 5. The following physical variables were simulated with the CTIP model: (a) electron density indicated as NmF2 (in m^{-3}), (b) neutral gas temperature indicated as T_n (in K), (c) meridional wind velocity vector where the magnitude is indicated as Vn_lat (in m/s) and the direction is ± equatorward/poleward; the arrows are wind velocity vectors: In the top right corner the vertical Vn arrow indicates the wind velocity in the north–south direction. Its maximum and minimum amplitude values are also stated, (d) upwelling indicated as Vn_IP (in m/s), (e) F2 layer height indicated as HmF2 (in km), (f) N_2 concentration indicated as N_N2 (in m^{-3}), (g) O_2 concentration indicated as N_O2 (in m^{-3}), and (h) O/N_2 ratio indicated as O/N2. At 0712:00 UT or ~2100 LT on the quiet day of 9 January, high electron densities (Figure 5a), high temperatures (Figure 5b), strong equatorward meridional winds (Figure 5c), strong upwellings (Figure 5d), maximum F2 layer heights (Figure 5e), medium N_2 concentration (Figure 5f), medium O_2 concentration (Figure 5g), and low O/N_2 ratios (Figure 5h) were written by the CTIP simulations.

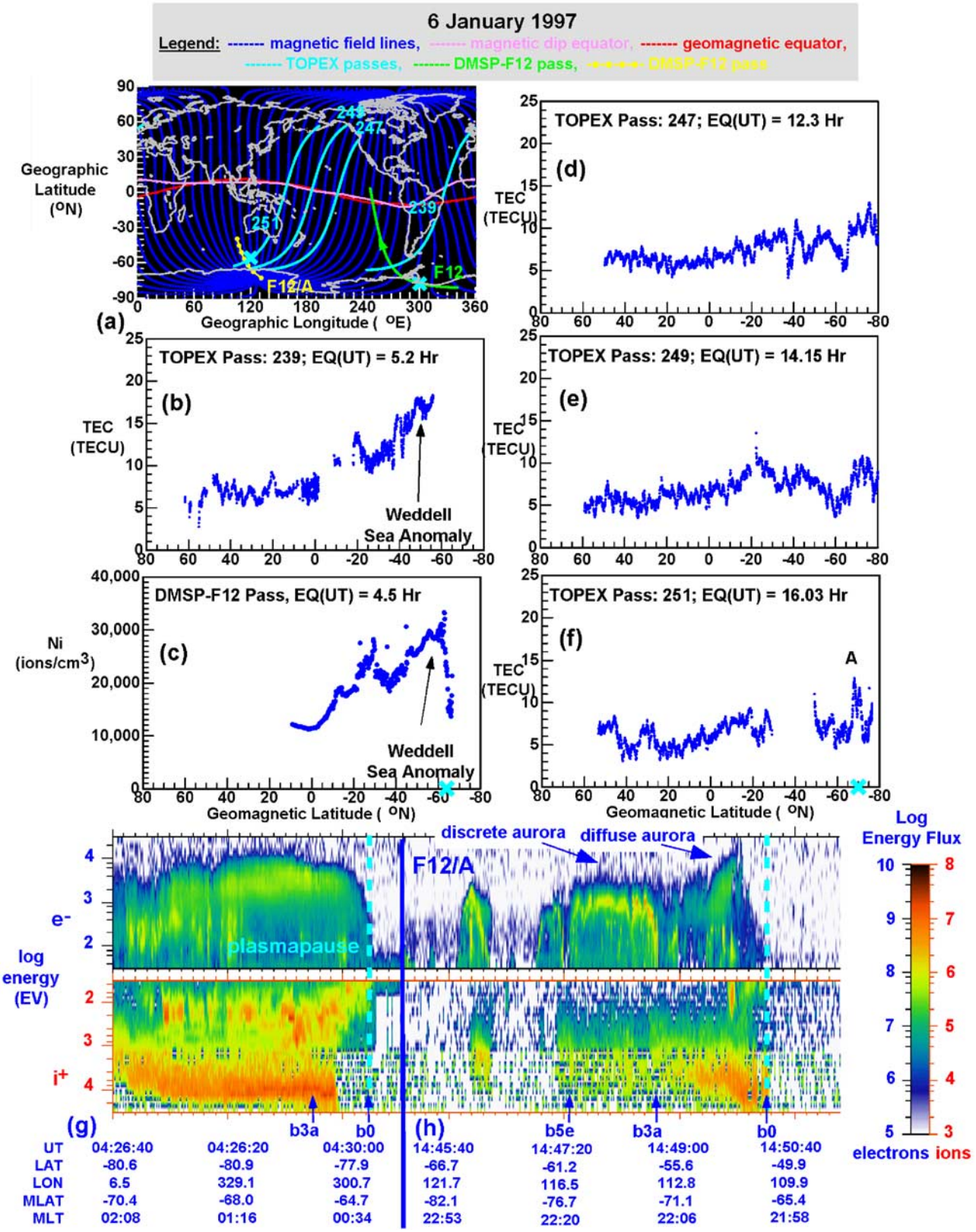
6 January 1997
Legend: magnetic field lines, magnetic dip equator, geomagnetic equator,
TOPEX passes, DMSP-F12 pass, DMSP-F12 pass
Geographic Latitude (°N)
Geographic Longitude (°E)
(a)
TOPEX Pass: 247; EQ(UT) = 12.3 Hr
(d)
TEC (TECU)
TOPEX Pass: 239; EQ(UT) = 5.2 Hr
(b)
Weddell Sea Anomaly
TOPEX Pass: 249; EQ(UT) = 14.15 Hr
(e)
DMSP-F12 Pass, EQ(UT) = 4.5 Hr
(c)
Ni (ions/cm3)
Geomagnetic Latitude (°N)
TOPEX Pass: 251; EQ(UT) = 16.03 Hr
(f)
A
discrete aurora
diffuse aurora
F12/A
plasmapause
e-
i+
log energy (EV)
Log Energy Flux
electrons ions
(g)
(h)
b3a
b0
b5e
UT 04:26:40 04:26:20 04:30:00 14:45:40 14:47:20 14:49:00 14:50:40
LAT -80.6 -80.9 -77.9 -66.7 -61.2 -55.6 -49.9
LON 6.5 329.1 300.7 121.7 116.5 112.8 109.9
MLAT -70.4 -68.0 -64.7 -82.1 -76.7 -71.1 -65.4
MLT 02:08 01:16 00:34 22:53 22:20 22:06 21:58

Figure 6

TEC decrease. This sudden decrease of the low-latitude TEC suggests that the magnetospheric convection electric field played an important role during this period of the storm main phase in the distribution of equatorial and lower midlatitude electron densities. Before the onset of main phase, B_Z turned northward (at ~0300 UT) and soon after that southward, and the enhanced westward electric field penetrated to the ionosphere before the shielding built up [*Ho et al.*, 1998]. In the nighttime sector generally, the downward E × B plasma drift, arising from the interaction of westward electric field (E) and magnetic field (B), pushes the plasma down to lower altitudes where the recombination rates are high and therefore lowers the equatorial and lower midlatitude TEC. In the premidnight sector, the depletion of low-latitude region indicated that the magnetospheric convection electric field, which was westward directed, played an important role in lowering the TEC. At around 0740 UT on 10 January, the second westward electric field penetration event occurred [*Ho et al.*, 1998]. This event didn't have an apparent interplanetary magnetic field trigger, but corresponded to the strong and steady southward B_Z, while the Dst (−78 nT) and *Kp* (6) indices were strongest and the AE index had a subpeak (1437 nT; see Figure 2). Thus this event corresponded to the strong geomagnetic disturbances (indicated by the Dst index) and also to a large potential drop across the polar cap (as seen as a subpeak in the AE index). The associated Joule heating event launched a traveling atmospheric disturbance. In the nighttime sector, the second intensification of downward E × B plasma drift further lowered the TEC to 5 TECU at equatorial latitudes (see Figure 7d).

[28] Meanwhile, in the Northern Hemisphere, some high-latitude enhancements, broken from the subauroral band and moved equatorward [*Ho et al.*, 1998], were detected at lower latitudes by TOPEX. Their ionospheric signature appearing as strong TEC enhancements (indicated as "E") relative to the background ionization can be seen in Figure 7. These features appeared first at around 36°N (geographic) and later at around 23°N, close to the American east coast and over Florida, respectively (see Figure 7a). Two TEC line plots show them in geomagnetic latitudes in Figures 7b–7c. Their movement to lower latitudes suggests the existence of atmospheric gravity waves. During the passage of gravity waves, the ionospheric plasma is being forced along the magnetic field lines by the neutral air winds driven by pressure waves. Enhanced electric fields produce a family of gravity-wave disturbances in the thermosphere that propagate preferentially in the meridional direction. Gravity-wave-like disturbances originate in the auroral region, particularly during magnetic storms. Thus they travel from the polar region toward the equator and are strongly correlated with magnetic storms [*Balthazor and Moffett*, 1997].

5.3.2. Recovery Phase

[29] At around the start of the recovery phase (1200 UT), TOPEX detected a subauroral enhancement (indicated as "E" in Figure 7d) in the Northern Hemisphere at around 45°N (geomagnetic). In the meantime, a complex electron density enhancement (indicated as "E" in Figure 7d) and the ionospheric signature of discrete aurora (indicated as 'A' in Figure 7d) were observed in the Southern Hemisphere. As the TOPEX pass was closely aligned to one of the magnetic field lines between equatorial and southern midlatitudes, it provided a so-called field-aligned TEC profile of that complex nighttime enhancement possibly created by strong equatorward blowing neutral winds. Its noticeable features are the sudden TEC drop-offs comprising its northern (at 20°S; geomagnetic) and southern (50°S) boundaries situated at 45°S and 65°S dip latitudes, respectively (dip angles are not shown in this study) where the meridional neutral winds were most efficient. On the basis of the corresponding DMSP spectrogram (see Figure 7k), the subauroral enhancement detected by TOPEX (indicated as "A" in Figure 7d) is the TEC signature of discrete and diffuse auroras, and the southern TEC drop-off is the signature of the plasmapause. Observed in Figures 7e–7g and indicated as "P", some southern enhancements (~23 TECU) peaking at around 25–30°S (geomagnetic) latitudes form the well-developed southern crest of an equatorial anomaly in the Australian longitude sector, and are the signature of fountain effect, indicating an eastward electric field.

[30] During the recovery phase, some repeated intensification of the aurora between 1400 UT and 1900 UT was recorded (see Figure 2). These surges of aurora were triggered by substorms and caused the development of ionization subpeaks appearing at subauroral latitudes on the poleward side of the plasmapause. Their ionospheric signatures were observed in the TOPEX TEC data (indicated as "A" in Figures 7e–7g), and were classified as discrete and diffuse auroras on the basis of the DMSP spectrograms (see Figures 7k–7m). Since the TOPEX passes of Figures 7e–7g) are not aligned to the magnetic field lines, the TEC drop-offs indicating the plasmapause, are not so well pronounced as before in Figure 7d. A TOPEX pass in Figure 7g, with a 45–60°S (geographic) section situated almost perpendicular to the magnetic field lines, shows the plasmapause least pronounced. Meanwhile, in the northern Hemisphere the previously observed subauroral peaks moved equatorward to 16°N (geomagnetic; see Figures 7f–7g) and to 10°N (see Figure 7h). This movement, indicating gravity waves during the recovery phase, left the higher midlatitude regions depleted.

[31] Marking the onset of a negative storm phase, there was a noticeable decrease in low- and midlatitude TEC after 1900 UT. Over the Indian Ocean, the peak (indicated as "P" in Figure 7h) reached only 13 TECU, which is a 56% TEC decrease with respect to the previous 23 TECU value (see

Figure 6. (a) The global map shows the ground tracks of some TOPEX and DMSP-F12 passes with the magnetic field lines and different equators. During the magnetically quiet time of 6 January 1997 a set of line plots illustrate the nighttime Weddell Sea Anomaly detected by TOPEX (b), its poleward boundary detected by the F12 spacecraft (c), and the nighttime ionosphere detected by TOPEX (d)–(f). Equator-crossing UT (indicated as EQ(UT)) is specified for each pass. Two DMSP-F12 spectrograms reveal the plasmapause indicated as b0 on the poleward side of the nighttime Weddell Sea Anomaly (g) and some discrete and diffuse auroras with the plasmapause in the Australian longitude region (h). The discrete aurora boundaries are marked as b3a (equatorward boundary) and b5e (poleward boundary).

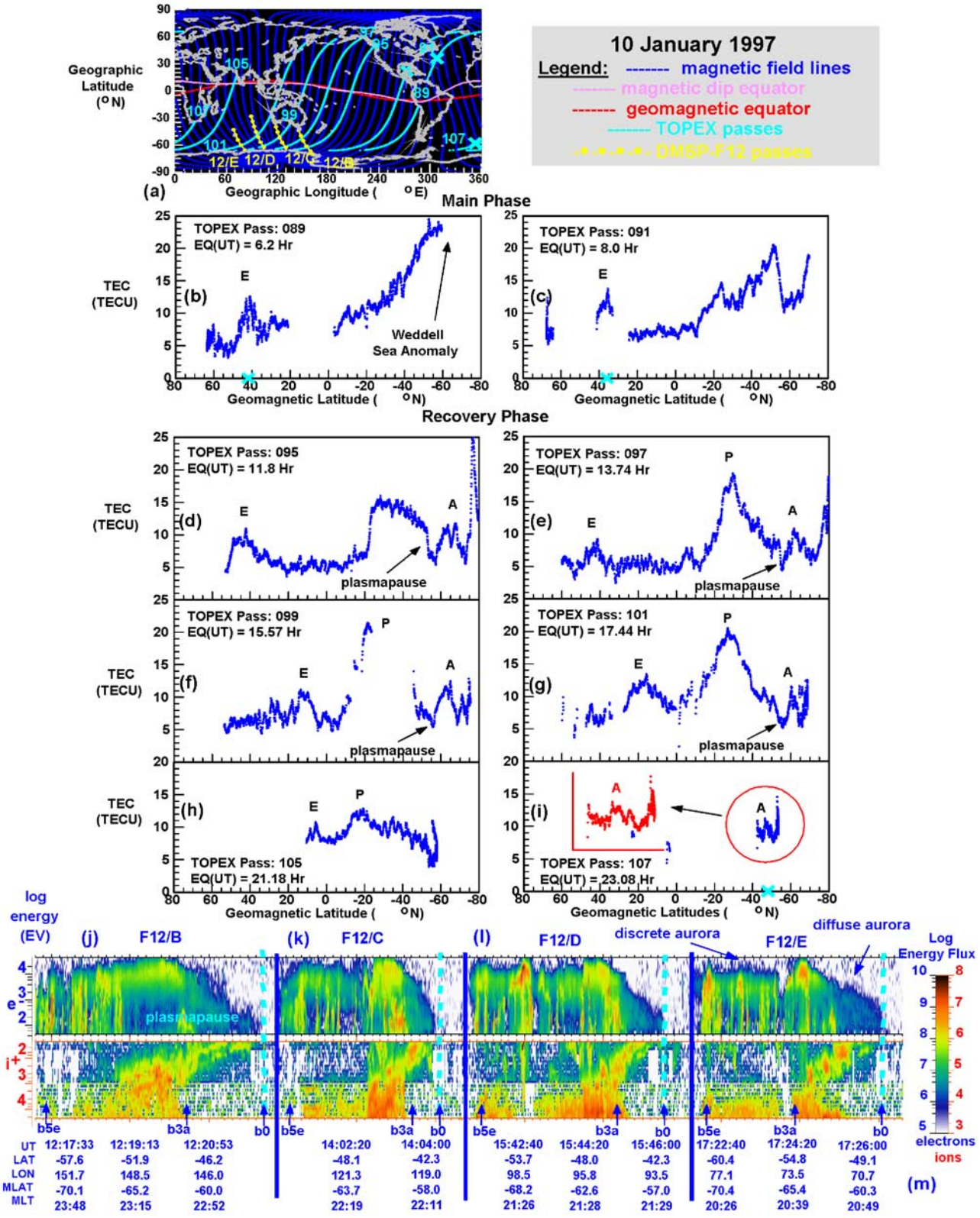

Figure 7. (top) (a) The global map shows the ground tracks of some TOPEX and DMSP-F12 passes with the magnetic field lines and different equators. (b)–(i): A set of TOPEX TEC line plots illustrate the various space weather features such as plasma enhancements (indicated as E), plasma peaks (indicated as P), and aurora enhancements (indicated as A) that developed during the 10 January magnetic storm. (bottom) (j)–(m) A series of DMSP-F12 spectrograms show some discrete and diffuse auroras with the plasmapause, confirming that their ionospheric signatures were observed in the TOPEX TEC data displayed in Figure 7 (top).

Figure 7g). At around 2300 UT over the southern Atlantic, a smaller auroral enhancement (indicated as "A" in Figure 7i) broke off from the subauroral band and drifted to lower latitudes similarly to its conjugate pair that was detected earlier in the Northern Hemisphere (see Figure 7b). The significance of this TOPEX pass 107, detecting this smaller auroral enhancement, is that it crossed the magnetic field lines perpendicularly. During that time, it became aligned almost parallel to the magnetic equator. Thus the end section of the TOPEX pass 107 provided a magnetically aligned TEC cross section of that auroral enhancement.

[32] As both the recovery phase and the negative storm phase continued on the following day, 11 January, the depletion of the entire nighttime Weddell Sea Anomaly was obviously strong (see Figure 8). During the first 5 hours in UT, its peak value dropped down to 12 TECU (see Figure 8b) and 15 TECU (see Figures 8c–8d) across the southwestern Atlantic and southeastern Pacific oceans, respectively. These TEC reductions indicate corresponding TEC decreases of 40% and 25% with respect to the 20 TECU peak value observed during the normal period of 9 January. With a TOPEX pass crossing the magnetic field lines, Figure 8d shows some periodic TEC variations. Further, at around 35°N (geomagnetic) and 7°N (see Figure 8e), along the east coast of southern United States and Mexico, some well-developed enhancements, probably traveling ionospheric disturbances (TIDs), appeared. It is noted here that as TIDs are the ionospheric signatures of gravity waves, TIDs do not propagate, only gravity waves propagate [*Balthazor and Moffett*, 1997]. In Figure 8e their waveforms, exhibiting an oscillatory character, comprise two cycles with a strong attenuation. These features are well indicated by the TOPEX pass 117 that was aligned quite closely to the magnetic field lines at northern middle and low latitudes. Later in time, some individual TEC peaks formed a strong positive storm phase across the South Pacific. This extended to the Australian east coast in the form of one single peak that was centered at ~45°S dip latitude (not shown) where the equatorward directed neutral winds were most effective. Increasingly aligned with the magnetic field lines at midlatitudes, the TOPEX passes 117, 119 and 123 (see Figures 8e–8g) show the true latitudinal cross sections of this single peak formation. According to some DMSP Ni observations (not shown in this paper but a good example can be viewed in the work of Horvath, unpublished manuscript, 2007b), the low-latitude spikes detected by the TOPEX satellite (see Figure 8f) are the ionospheric signature of strong upward plasma drifts indicating intensive equatorward neutral winds. A strong auroral surge triggered the development of a substorm at around 1200 UT. At around 1300 UT, a DMSP-F12 pass detected some discrete and diffuse auroras. Their ionospheric signature, indicated as "A" in Figure 8g, was also seen in the TOPEX TEC data.

6. Discussion

6.1. CTIP-Modeled Positive and Negative Storm Phases

[33] The prompt penetration of high-latitude electric fields to lower latitudes is most likely associated with ionospheric disturbance dynamo effects produced by the enhanced energy deposition into the auroral ionosphere during magnetic storms [*Blanc and Richmond*, 1980]. This event can occur before opposing shielding effects in the inner magnetosphere build up [*Gonzales et al.*, 1983; *Sastri et al.*, 1992]. On the ionospheric plasma densities, the most obvious effects of penetration electric fields are the positive and negative storm phases appearing as increases and decreases relative to the quiet time conditions, respectively. Illustrated in Figure 3 with TOPEX TEC and DMSP-F12 Ni maps, this study's experimental results show the quiet time nighttime ionosphere and its response to the 6–11 January events. A strong asymmetric nighttime plasma distribution about the magnetic equator and a typical nocturnal F2 region storm pattern, where the nighttime Weddell Sea Anomaly and the ionosphere in the Australian longitude sector exhibited the most dramatic TEC variations in the southern ionosphere, are the most obvious features of these TEC and Ni maps.

[34] The formation of positive and negative storm phases involves several mechanisms. The most probable ones to consider for positive storm phases are (1) the F2 layer uplift, caused either by an increased eastward electric field of magnetospheric origin or by an equatorward horizontal thermospheric circulation, lifting up the F2 layer along the inclined magnetic field lines, (2) plasma fluxes from the plasmasphere, and (3) downwellings resulting from strong storm-induced thermospheric circulations [*Proelss*, 1993]. During magnetically quiet periods, the F2 layer peak height (hmF2) tends to lie near a constant pressure level in the thermosphere [*Rishbeth and Edwards*, 1989]. At peak F2 layer altitude, the electron concentration and TEC is directly proportional to the ratio of O and N_2 concentrations (i.e., $[O]/[N_2]$; *Mikhailov et al.* [1995]). Thermospheric neutral winds can move the F2 layer above or below this level. The lifting of the F2 layer to regions of reduced loss, while production is still occurring, can produce electron density and TEC increases, and thus positive phases. An equatorward downwelling, through constant pressure surfaces, naturally increases the electron concentration and TEC by decreasing $[N_2]$ and $[O_2]$ concentrations, causing the ionosphere to decay more slowly and the TEC to remain higher. It is generally believed that a negative storm phase can be caused by a change in the neutral gas composition (i.e., $[O]/[N_2]$ ratio) because of the heating of the lower part of the thermosphere in the auroral region. This heating leads to the immediate depletion of the atoms-to-molecules or $[O]/[N_2]$ ratio. Since the electron concentration and TEC are directly proportional to this ratio at F2 layer heights, the immediate depletion of $[O]/[N_2]$ ratio also means an immediate depletion of TEC.

[35] To get a better insight into the development of positive and negative phases taking place in the Weddell Sea Anomaly region, some further CTIP simulations were generated for the days of 10 and 11 January. These simulations are the continuation of the quiet time modeling efforts carried out for 9 January (see Figure 5). To explain the development of positive and negative storm phases that were so obviously shown by the nighttime Weddell Sea Anomaly at ~0700 UT on 10 and 11 January, respectively, the same set of physical variables that were run for 9 January (see Figure 5) were generated for 10 January (see Figure 9) and 11 January (see Figure 10). It is mentioned again that CTIP simulations made

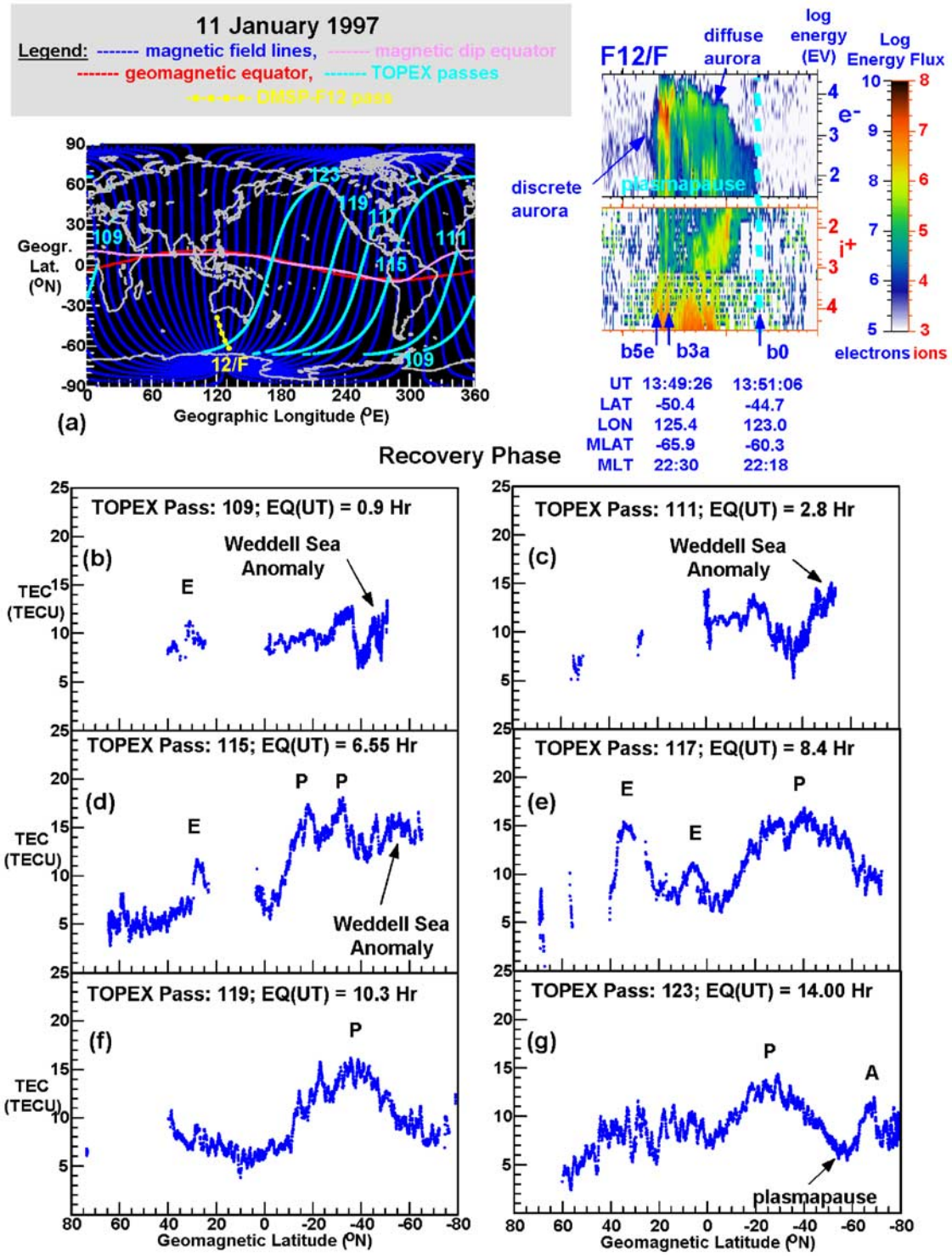

Figure 8. (a) The global map shows the ground tracks of some TOPEX passes and a DMSP-F12 pass with the magnetic field lines and different equators. (b)–(g) A set of TOPEX TEC line plots illustrate the nighttime Weddell Sea Anomaly and other space weather features such as plasma enhancement (E), plasma peaks (P), and auroral enhancements (A) during the recovery phase of the 10 January storm. In the top right corner, the DMSP-F12 spectrogram shows some discrete and diffuse auroras with the plasmapause, confirming that their ionospheric signatures were observed in the TOPEX TEC data of pass 123 displayed in Figure 8g.

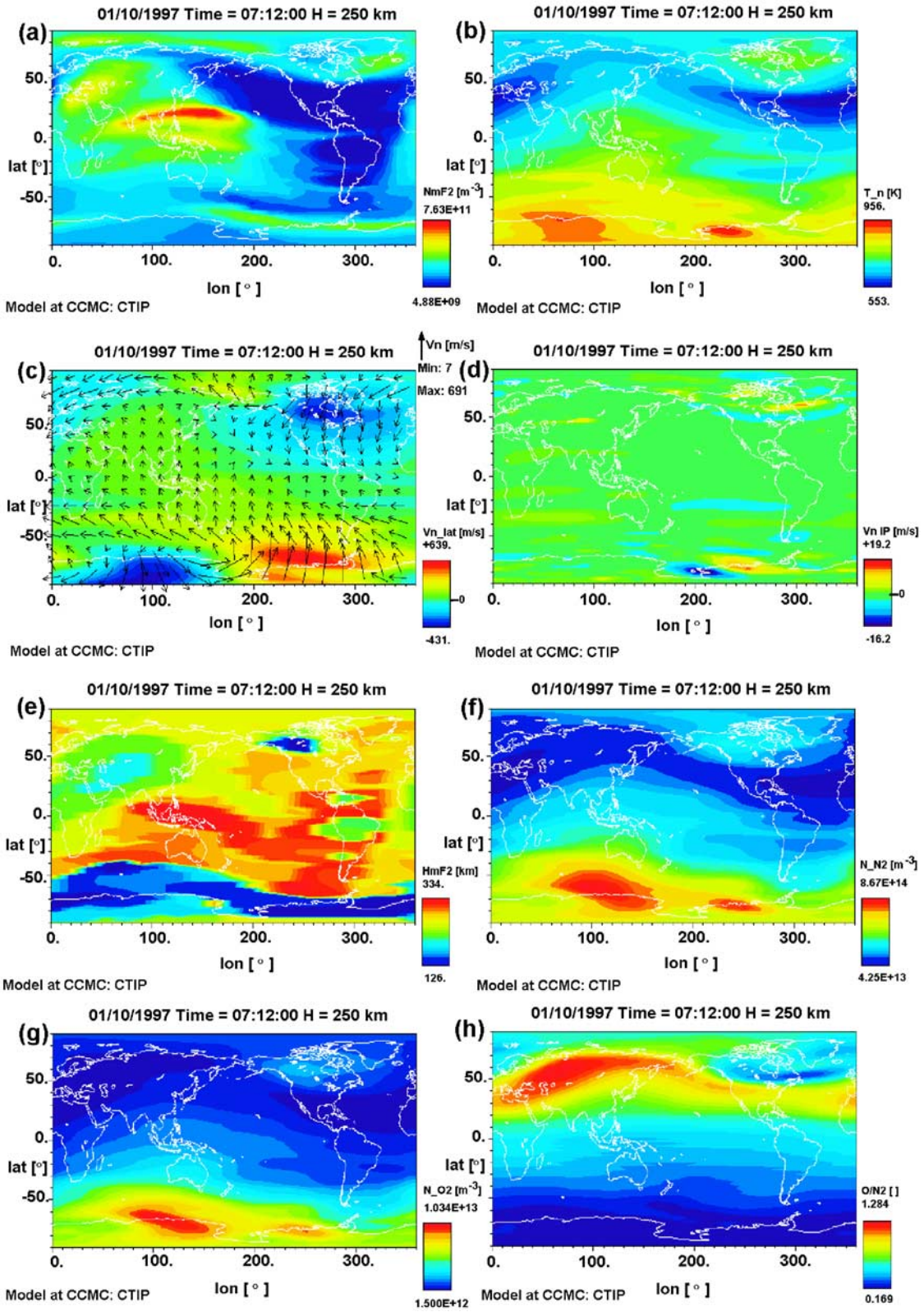

Figure 9. On 10 January 1997, at 0712:00 UT (~2100 LT), during the main phase of the 10 January storm close to maximum electron densities (a), maximum temperatures (b), maximum equatorward meridional winds (c), maximum upwellings (d), maximum F2 layer heights (e), maximum N_2 concentrations (f), high O_2 concentrations (g), and minimum O/N_2 ratios (h) were written by the CTIP simulations for the center of the nighttime Weddell Sea Anomaly situated in the high midlatitude region of the 230–250°E longitude sector.

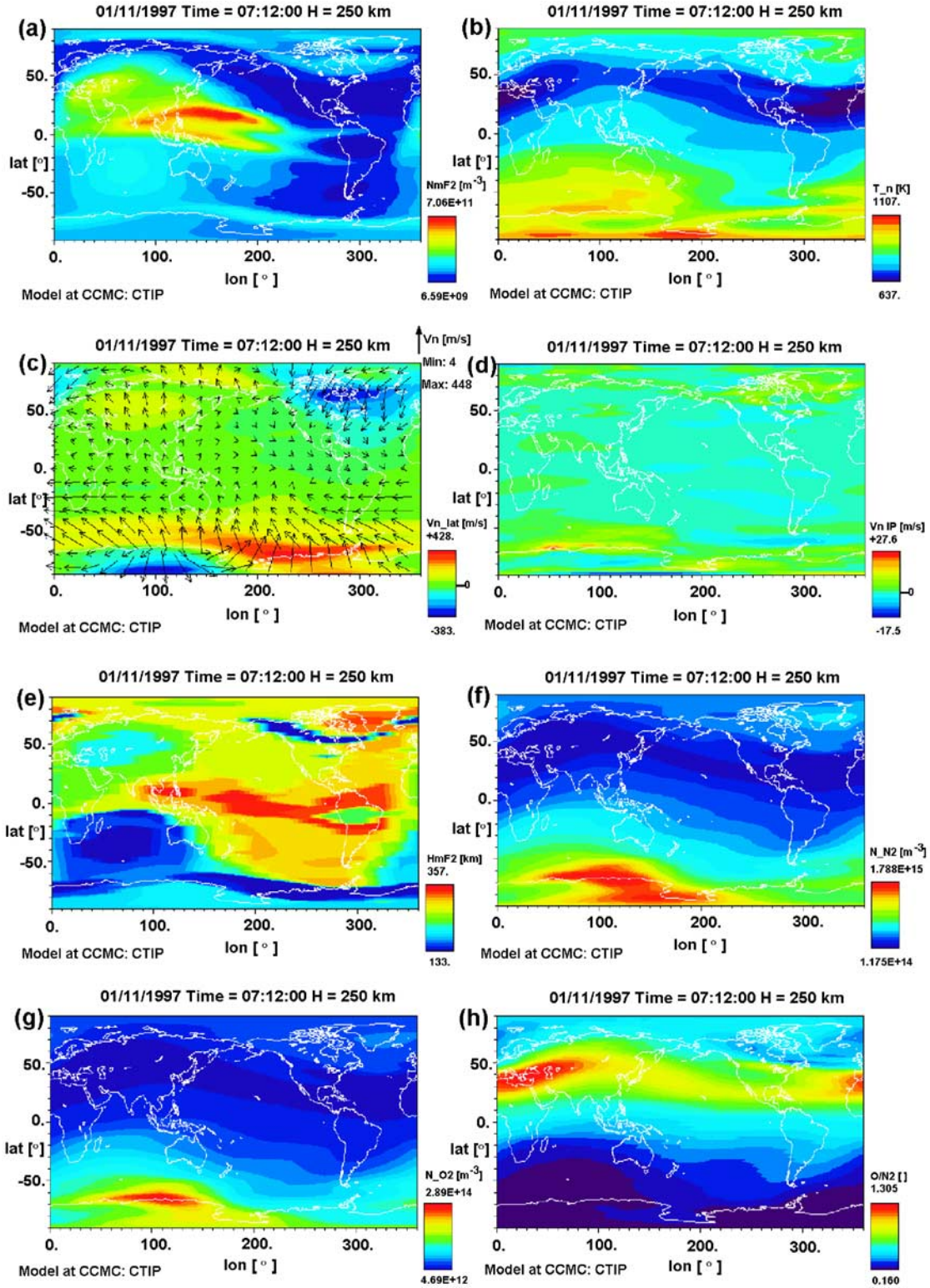

Figure 10. On 11 January 1997, at 0712:00 UT (~2100 LT), during the recovery phase of the 10 January storm, medium electron densities (a), medium temperatures (b), maximum equatorward meridional winds (c), medium upwellings (d), high F2 layer heights (e), medium N_2 concentrations (f), low O_2 concentrations (g), and minimum O/N_2 ratios (h) were written by the CTIP simulations for the center of the nighttime Weddell Sea Anomaly situated in the high midlatitude region of the 230–250°E longitude sector.

for the center of the Weddell Sea Anomaly detected at ~0700 UT are displayed by the high midlatitude region of the ~230–250°E (geographic) longitude sector on each map. In Figure 9a, the increased NmF2 indicates the intensification of the Weddell Sea Anomaly, which is the signature of a positive storm phase. At that time, the high temperatures peaking at the center of the nighttime Weddell Sea Anomaly suggest increased high-latitude heating (see Figure 9b), which generated stronger equatorward directed neutral winds (see Figure 9c) and upwellings (see Figure 9d) compared with the quiet time values. The combination of strong winds and upwellings lifted the F2 layer to greater heights (see Figure 9e) where the loss rates were lower, and thus helped to increase the N_2 (see Figure 9f) and O_2 (see Figure 9g) concentrations leading to a decreases in the O/N_2 ratios (see Figure 9h). On the following day, 11 January, the development of a negative phase was indicated by the sudden depletion of F2 layer electron densities (see Figure 10a). Increased heating (see Figure 10b) coupled with weaker equatorward directed neutral winds (see Figure 10c) created weaker upwellings (see Figure 10d). Thus the F layer rise was moderate (see Figure 10e). However, a change in the chemical makeup of neutral air was greater. An increased N_2 concentration (see Figure 10f) and a decreased O_2 concentration (see Figure 10g) reduced significantly the O/N_2 ratio (see Figure 10h) giving rise to the significant depletion of electron concentration and thus the development of a negative phase.

6.2. Long-Duration Positive Storm Effects Experienced by the Nighttime Weddell Sea Anomaly

[36] A set of experimental data from DMSP-F12 in situ plasma measurements was utilized to investigate the actual physical processes that took place during the positive phase, and to test the validity of CTIP simulations. Described below, the analysis of experimental data carried out in the light of current theories revealed that the nighttime Weddell Sea Anomaly experienced long-duration positive storm effects during the 10 January storm.

[37] From the magnetic data it is known that the onset and main storm phase lasted between 0440 and 0600 UT, and 0600 and 1000 UT, respectively. During those times, the nighttime Weddell Sea Anomaly exhibited a strong positive phase over the southeastern Pacific and southwestern Atlantic oceans. During this positive storm phase, the southern aurora intensified three times, each time subjecting the thermosphere to significant heating of which the main sources were the Joule dissipation of the currents plus a smaller input provided by absorption of the precipitating particles. Usually, these heating processes induce their own circulation that is equatorward directed at F2 layer altitudes. These heating processes also connect with the regular background circulation that is equatorward directed at nighttime in any season and at all times during summer. During summer nights, when the background and storm-induced circulations are all equatorward directed, these circulations coincide. As the space-based DMSP data indicate, that was the case during the January storm.

[38] To demonstrate the significance of the *above mentioned* coinciding circulations, the response of various ionospheric parameters to the positive storm effects are illustrated in Figure 11. Two sets of DMSP plots, one for the quiet day of 6 January (see first column of Figure 11) and one for the main storm phase taking place on 10 January (see second column of Figure 11), were constructed. A period of 0500–0600 UT when the DMSP-F12 spacecraft passed over the center of nighttime Weddell Sea Anomaly was chosen. During that time, the DMSP-F12 spacecraft detected a normal smaller plasma density peak (~28,000 ions/cm^3; see Figure 11b) of the nighttime Weddell Sea Anomaly on the magnetically quiet day of 6 January. During the main storm phase of 10 January, the peak plasma density increased to 54,497 ions/cm^3, see Figure 11f) indicating a ~50% increase in Ni. Simultaneously with the plasma density increase there was also a sudden increase in $[O^+]$ toward the Weddell Sea Anomaly peak on both days (6 and 10 January, see Figures 11e and 11i, respectively). Whilst $[O^+]$ remained sustained over higher latitudes, there was a sudden jump in both electron (Te; from 3,800°K to 4,800°K) and ion (Ti; from 3,000°K to 3,600°K) temperatures (see Figures 11c and 11g) at around 63°S (geomagnetic), where the plasma density peaked. As the concentrations of O^+ and H^+ are controlled by the charge exchange reaction of $O^+ + H \rightleftarrows O + H^+$ [*Denton et al.*, 2002] between them, the O^+ and H^+ curves in Figure 11 are mirror images. In the Weddell Sea Anomaly region, under normal magnetic activity (6 January), the high Te and Ti values at 63°S (geomagnetic) and higher latitudes indicate a heat source generated by the solar illumination of the F2 layer. Under the magnetic disturbance of 10 January, the intensification of aurora created an additional heat source, which explains the higher temperatures attained during that day. At around 63°S, there was also a sudden increase in the upward vertical plasma flux, computed as $V_Z \cdot Ni$ where V_Z is the upward plasma drift velocity, indicating the strongest upward plasma drift (~4000 ions/(s cm^2); see Figure 11d) at the center of Weddell Sea Anomaly. During the main phase, a much stronger upward plasma flux (~4900 ions/(s cm^2); see Figure 11h, indicating a 22.5% increase in upward plasma flux) was detected over the same location. Increased plasma drifts and plasma fluxes during the positive phase indicate that the combined circulations (storm time and quiet time) created a stronger vertical upward drift, which led to the formation of a positive phase in the Weddell Sea Anomaly region. There, the sunlit ionosphere and the nighttime equatorward winds were the most effective geophysical factors responsible for maintaining high solar-produced ionization levels, while production was still occurring and therefore keeping the $[O^+]$ high because of the easterly declination patterns. Thus a well pronounced positive phase was created that became maintained during the main storm phase. *Proelss* [1997] called the above described mechanisms long-duration positive storm effects. In good agreement with the experimental DMSP results, the CTIP simulations indicated the same underlying physical mechanisms characterizing the long-duration positive storm effects.

6.3. Particularly Strong Negative Storm Effects Experienced by the Nighttime Weddell Sea Anomaly

[39] In the third column of Figure 11, a set of in situ plasma measurements recorded by the DMSP-F12 spacecraft on 11 January was utilized to investigate the actual physical processes that took place during the negative storm phase, and to test the validity of CTIP simulations. An analysis of experimental data, carried out according to our

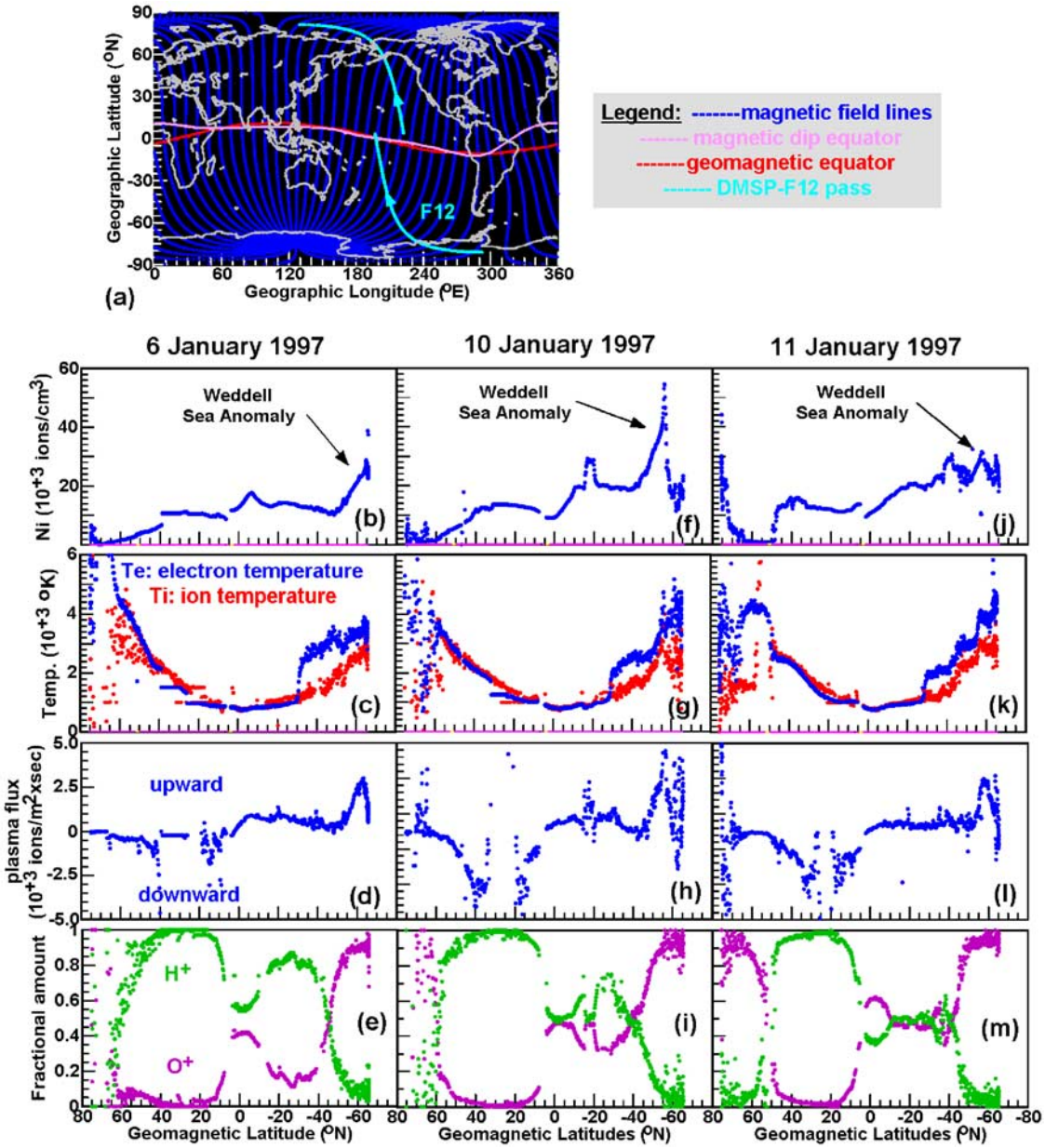

Figure 11. (a) The global map shows a ground track of F12 spacecraft. A series of multi-instrument DMSP-F12 observations such as ion density (Ni), ion and electron temperatures (Ti and Te), plasma flux, and chemical compositions (O^+ and H^+) are utilized to learn about the nighttime ionosphere's and Weddell Sea Anomaly's plasma environments under magnetically quiet (1st column) and magnetically disturbed (2nd column during the positive phase and 3rd column during the negative phase) conditions created by the 6–11 January events.

current understanding, revealed that the nighttime Weddell Sea Anomaly experienced particularly strong negative storm effects on 11 January.

[40] According to current understanding, a negative storm phase is triggered by the divergent nature of the winds causing upwelling of molecular rich thermospheric gas from lower altitudes. This upwelling is caused by the heating of the lower part of the thermosphere, at around 100–140 km, in the auroral region. In both hemispheres, elevated temperatures were recorded by DMSP-F12 (see Figure 11k). Whilst the Ti and Te temperatures increased gradually in the Weddell Sea Anomaly region, there was a well defined high-latitude thermal (Te) bulge in the Northern Hemisphere. Their main heat source was the Joule dissipation of currents and the absorption of precipitating particles [*Proelss*, 1993] in the northern Hemisphere, and the solar illumination in the Weddell Sea Anomaly region. It is well known today that at *F* region altitudes the enhanced molecular species create so-called composition bulges that are transported by both the preexisting background quiet time circulations and the storm-induced wind circulations. Later in time, the changed composition feeds back to the

ionosphere [*Fuller-Rowell et al.*, 1996a]. In the two hemispheres, the Joule heating varies significantly because of the large differences in conductivity. During the nighttime darkness in the northern ionosphere, the Pedersen conductivity is significantly lower than in the sunlit Weddell Sea Anomaly region [*Rodger et al.*, 1989]. Thus the heating rates are larger in the Weddell Sea Anomaly region (see Ti and Te curves in Figure 11k) and the elevated temperatures encompass a wider latitude range than in the Northern Hemisphere or elsewhere in the Southern Hemisphere.

[41] Because of the thermal expansion of the upper atmosphere, caused by the heating, the ratio of $[O]/[N_2]$ throughout the entire thermosphere in the auroral region is immediately reduced. By assuming that other chemical conditions remain unchanged, the decrease of $[O]/[N_2]$ suggests a decrease in plasma density and TEC at F2 layer heights [*Proelss*, 1980; *Proelss and von Zahn*, 1997]. DMSP-F12 detected this plasma density reduction in the Weddell Sea Anomaly region (see Figure 11j): Ni dropped down to ~30,000 ions/cm^3 (see Figure 11j) indicating a ~50% Ni decrease with respect to the previous day's value. Because of the already low northern plasma densities (~2000 ions/cm^3) due to the nighttime darkness, there is little decrease at high latitudes but the Ni decrease is more dramatic at ~50°N (geomagnetic) latitude indicated by a sudden plasma density drop-off. Because of the still strong upward plasma flux (~4000 ions/(s cm^2); see Figure 11l) and to the still continuous ion production because of the sunlit F2 layer in the Weddell Sea Anomaly region, the southern plasma densities are still high during this negative phase compared with other latitude regions in the Northern Hemisphere or elsewhere in the Southern Hemisphere. High concentrations of O^+ in the Northern Hemisphere are due to particle precipitation, while in the Weddell Sea Anomaly region the direct photoionization is the main source. Increased N_2 concentrations, not measured by DMSP, were responsible for the significant reduction of O/N_2 ratios that are proportional to the plasma densities. Modeled accurately by CTIP, the variation of simulated O/N_2 ratios reflected this sudden decrease during the negative phase. During summer, the quiet time background circulation coincides with the storm-induced circulation. Then, the development of a negative storm phase becomes even more intense because of the greater composition changes (i.e., O/N_2 decrease) occurring in the sunlit F2 layer. According to these geophysical factors, the nighttime Weddell Sea Anomaly was subjected to particularly strong negative storm effects during the January storm. Changes occurring in the thermospheric composition, because of the heating of the thermosphere during geomagnetic disturbances, were first realized by *Seaton* [1956].

7. Summary and Conclusion

[42] Delivered by a geomagnetic storm, some large energy inputs to the upper atmosphere resulted in the development of the 10 January 1997 ionospheric storm. These magnetic events were triggered by the impact of an interplanetary shock wave that was launched by a coronal mass ejection 4 days before, on 6 January. Those large energy inputs took the form of enhanced electric fields, currents, and energetic particle precipitation. According to our current understanding, the major drivers of the underlying physical mechanisms were the following: Electric fields penetrated into lower latitudes and caused the development of positive and negative storm phases via the interaction of high-latitude electric fields and increased storm-time ring currents; the auroral zone expanded into midlatitudes and produced excess ionization; and traveling atmospheric disturbances (TADs), propagating from high to equatorial latitudes, launched traveling ionospheric disturbances (TIDs).

[43] By combining multi-instrument measurements with CTIP simulations, space weather changes of the nighttime ionosphere were tracked down, and the underlying physical and chemical processes were explained. Experimental results revealed the quiet time plasma distribution of the nighttime ionosphere characterized by a well developed Weddell Sea Anomaly. Similar quiet time ionospheric structures were simulated by the Bent model. In the high midlatitude region, west of the American longitude sector, the CTIP generated quiet time NmF2 map clearly indicated the existence of a nighttime Weddell Sea Anomaly. According to experimental results, there was a strong reaction triggered from the nighttime Weddell Sea Anomaly by the January events. Storm-time responses were exhibited by the anomaly's intensification during the storm main phase and by its depletion during the recovery phase. Other interesting storm-related features such as high and midlatitude plasma enhancements and TIDs were also demonstrated. While the Bent model could not reproduce any storm-related ionospheric response, the various physical variables written by CTIP provided a better insight into the underlying chemical and physical processes. From the obtained experimental and modeling results, the following storm effects were identified:

[44] 1. During the main phase, the nighttime Weddell Sea Anomaly experienced long-duration positive storm effects (~50% increase in TEC and Ni) decreasing the O/N_2 ratio.

[45] 2. During the recovery phase, the nighttime Weddell Sea Anomaly experienced particularly strong negative storm effects (~45% decrease in TEC and ~50% decrease in Ni) causing the sudden and dramatic depletion of the O/N_2 ratio.

[46] 3. During the recovery phase, a particularly strong plasma enhancement developed between dip latitudes of 45°S and 65°S where the equatorward winds are usually most effective. At ~60°S (geomagnetic) the sudden TEC drop-off, which is the signature of the plasmapause, formed the southern boundary.

[47] 4. During the recovery phase, some well formed enhancements (possibly TIDs), exhibiting waveforms of an oscillatory character and a strong attenuation over two cycles, were detected in the TOPEX TEC data.

[48] 5. During the recovery phase, the effects of Joule heating produced a well-defined thermal bulge and enhanced $[O^+]$ creating a composition bulge in the Northern Hemisphere.

[49] 6. During the main and recovery phases, the effects of a stronger heat source made up of Joule heating and solar UV radiation were detected over a wider latitude range in the Weddell Sea Anomaly region.

[50] As a final remark, this paper is the first to report the response of the nighttime Weddell Sea Anomaly to a geomagnetic storm. The results listed in the first and last two points have not been reported in the published literature

before. Thus these findings are considered significant in that they contribute to the better understanding of ionospheric storm effects and thus move science forward.

[51] **Acknowledgments.** Ildiko Horvath is supported by a University of Queensland postdoctoral research fellowship. The author is thankful to the Wind and DMSP project teams for the data and to the Community Coordinated Modeling Center at NASA Goddard Space Flight Center for the CTIP model simulations. Simulation results have been provided by the Community Coordinated Modeling Center through their public Runs on Request system (http://ccmc.gsfc.nasa.gov). The CCMC is a multiagency partnership between NASA, AFMC, AFOSR, AFRL, AFWA, NOAA, NSF, and ONR. The CTIP model was developed by T. Fuller-Rowell at the Space Environment Center (NOAA SEC). Special thanks are extended to M. Hairston for his advice, to NOAA's Geophysical Data Center for the geomagnetic data. and to JPL for the TOPEX radar data. The TOPEX data were obtained from the NASA Physical Oceanography Distributed Active Archive Center and the Jet Propulsion Laboratory/California Institute of Technology.

[52] Zuvin Pu thanks the reviewer for assistance in evaluating this paper.

References

Balthazor, R. L., and R. J. Moffett (1997), A study of atmospheric gravity waves and traveling ionospheric disturbances at equatorial latitudes, *Ann. Geophys.*, *15*, 1048–1056.

Blanc, M., and A. D. Richmond (1980), The ionospheric disturbance dynamo, *J. Geophys. Res.*, *85*, 1669–1686.

Buonsanto, M. J. (1999), Ionospheric storms: A review, *Space Sci. Rev.*, *88*, 563–601.

Buonsanto, M. J., and T. J. Fuller-Rowell (1997), Strides made in understanding space weather at Earth, *Eos Trans. AGU*, *78*, 1–7.

Buonsanto, M. J., S. A. Gonzales, G. Lu, B. W. Reinish, and J. P. Thayer (1999), Coordinated incoherent scatter radar study of the January 1997 storm, *J. Geophys. Res.*, *104*, 24,625–24,637.

Davis, C. J., M. N. Wild, M. Lockwood, and Y. K. Tulunay (1997), Ionospheric and geomagnetic responses to changes in IMF B_Z: A superposed epoch study, *Ann. Geophys.*, *15*, 217–230.

Denton, M. H., G. J. Bailey, C. R. Wilford, A. S. Rodger, and S. Venkatraman (2002), He+ dominance in the plasmasphere during geomagnetically disturbed periods: 1. Observational results, *Ann. Geophys.*, *20*, 461–470.

Dudeney, J. R., and W. R. Piggott (1978), Antarctic ionospheric research, in *Upper Atmosphere Research in Antarctica*, *Antarct. Res. Ser.*, vol. 29, edited by L. J. Lanzerotti and C. G. Park, pp. 200–235, AGU, Washington, D. C.

Dungey, J. W. (1961), Interplanetary magnetic field and the auroral zones, *Phys. Rev. Lett.*, *6*, 47–48.

Fox, N. J., M. Peredo, and B. J. Thompson (1998), Cradle to grave tracking of the January 6–11, 1997 Sun-Earth connection event, *Geophys. Res. Lett.*, *25*, 2461–2464.

Fuller-Rowell, T. J., M. V. Codrescu, H. Rishbeth, R. J. Moffett, and S. Quegan (1996a), On the seasonal response of the thermosphere and ionosphere to geomagnetic storms, *J. Geophys. Res.*, *101*, 2343–2353.

Fuller-Rowell, T. J., D. Rees, S. Quegan, R. J. Moffett, M. V. Codrescu, and G. H. Millward (1996b), A coupled thermosphere-ionosphere model (CTIM), in *STEP Handbook of Ionospheric Models*, edited by R. W. Schunk, pp. 217–238, Utah State Univ., Logan, Utah.

Gonzales, C. A., M. C. Kelley, R. A. Behnke, J. F. Vickrey, R. Wand, and J. Holt (1983), On the latitudinal variations of the ionospheric electric field during magnetospheric disturbances, *J. Geophys. Res.*, *88*, 9135–9144.

Gosling, J. T. (1993), Coronal mass ejections: The link between solar and geomagnetic activity, *Phys. Fluids B*, *5*, 2638–2645.

Hairston, M. R., R. Heelis, and F. Rich (1997), Analysis of the ionospheric cross polar cap potential drop and polar ion convection patterns during the January 1997 CME events using DMSP data, *Eos Trans. AGU*, *78*(17), Spring Meet. Suppl., S264.

Harten, R., and K. Clark (1995), The design features of the GGS Wind and POLAR spacecraft, *Space Sci. Rev.*, *71*, 23–40.

Ho, C. M., A. J. Mannucci, U. J. Lindquister, X. Pi, B. T. Tsurutani, L. Sparks, B. A. Iijima, B. D. Wilson, I. Harris, and M. J. Reyes (1998), Global ionospheric TEC variations during January 10, 1997 storm, *Geophys. Res. Lett.*, *25*, 2589–2592.

Horvath, I. (2006), A total electron content space weather study of the nighttime Weddell Sea Anomaly of 1996/97 southern summer with TOPEX/Poseidon radar altimetry, *J. Geophys. Res.*, *111*, A12317, doi:10.1029/2006JA011679.

Horvath, I., and E. A. Essex (2003), The Weddell Sea Anomaly observed with the TOPEX satellite data, *J. Atmos. Sol. Terr. Phys.*, *65*, 693–706.

Imel, D. A. (1994), Evaluation of the TOPEX/Poseidon dual-frequency ionospheric correction, *J. Geophys. Res.*, *99*, 24,895–24,906.

Jakowski, N., S. Schluter, and E. Sardon (1999), Total electron content of the ionosphere during the geomagnetic storm on 10 January 1997, *J. Atmos. Sol. Terr. Phys.*, *60*, 299–307.

Lepping, R. P., et al. (1995), The Wind magnetic field investigation, *Space Sci. Rev.*, *71*, 207–229.

McEwen, D. J., D. P. Steele, F. Creutzberg, and D. D. Wallis (1999), The ionospheric response to the CME event of 6–11 January 1997, *J. Atmos. Sol. Terr. Phys.*, *61*, 223–232.

Mikhailov, A. V., and M. Forster (1999), Some F_2-layer effects during the January 06–11, 1997 CEDAR storm period as observed with the Millstone Hill incoherent scatter facility, *J. Atmos. Sol. Terr. Phys.*, *61*, 249–261.

Mikhailov, A. V., M. G. Skoblin, and M. Froster (1995), Daytime F-2 layer positive storm effect at middle and lower latitudes, *Ann. Geophys.*, *13*, 532.

Millward, G. H., R. J. Moffett, S. Quegan, T. J. Fuller-Rowell (1996), A Coupled Thermosphere-Ionosphere-Plasmasphere model (CTIP), in *STEP Handbook of Ionospheric Models*, edited by R. W. Schunk, pp. 239–279, Utah State Univ., Logan, Utah.

Newell, P. T., Y. I. Feldstein, Y. I. Galperin, and C.-I. Meng (1996), Morphology of nightside ionization, *J. Geophys. Res.*, *101*, 10,737–10,748.

Penndorf, R. (1965), The average ionospheric conditions over the Antarctic, in *Geomagnetism and Aeronomy*, *Antarct. Res. Ser.*, vol. 4, edited by A. H. Waynick, pp. 1–45, AGU, Washington, D. C.

Proelss, G. W. (1980), Magnetic storm associated perturbations of the upper atmosphere: Recent results obtained with satellite borne gas analyzers, *Rev. Geophys. Space Phys.*, *18*, 183–202.

Proelss, G. W. (1993), On explaining the local time variation of ionospheric storm effects, *Ann. Geophys.*, *11*, 1–9.

Proelss, G. W. (1997), Magnetic storm associated perturbations of the upper atmosphere, in *Magnetic Storms*, *Geophys. Monogr. Ser.*, vol. 98, edited by B. T. Tsurutani et al., pp. 227–241, AGU, Washington, D. C.

Proelss, G. W., and U. von Zahn (1997), On the global morphology of negative ionospheric storms, *Space Res.*, *17*, 433–438.

Rishbeth, H., and R. Edwards (1989), The Isobaric F2-layer, *J. Atmos. Terr. Phys.*, *51*, 321–338.

Rishbeth, H., I. C. F. Muller-Wodarg, I. Zou, T. J. Fuller-Rowell, G. H. Millward, R. J. Moffett, D. W. Idenden, and A. D. Alyward (2000), Annual and semiannual variations in the ionospheric F2-layer: II. Physical discussion, *Ann. Geophys.*, *18*, 945–956.

Rodger, A. S., G. L. Wrenn, and H. Rishbeth (1989), Geomagnetic storms in the Antarctic F-region: II. Physical interpretation, *J. Atmos. Terr. Phys.*, *51*, 851–866.

Rufenach, C. L., R. F. Martin Jr., and H. H. Sauer (1989), A study of geosynchronous magnetopause crossings, *J. Geophys. Res.*, *94*, 15,125–15,134.

Sastri, J. H., H. N. R. Rao, and K. B. Ramesh (1992), Response of equatorial ionosphere to the transit of interplanetary magnetic cloud of January 13–15 (1967), Transient disturbance in F region, *Planet. Space Sci.*, *40*, 519–534.

Seaton, M. J. (1956), A possible explanation of the drop in F-region critical densities accompanying major ionospheric storms, *J. Atmos. Terr. Phys.*, *8*, 122–124.

Smith, E. J., J. A. Slavin, R. D. Zwickl, and S. J. Bame (1986), Shocks and storm sudden commencements, in *Solar Wind-Magnetosphere Coupling*, edited by Y. Kamide and J. A. Slavin, pp. 345–365, Terra Sci., Tokyo.

I. Horvath, School of Information Technology and Electrical Engineering, Electromagnetics and Imaging, University of Queensland, Brisbane, QLD, 4072, Australia. (ihorvath@itee.uq.edu.au)